TopHat with that of BWA for an optimal alignment for each sequence read. The ambiguously mapped reads and the duplicates were excluded. The level of gene expression was calculated in reads per kilobase of exonic sequence per million aligned reads (RPKM).

Mutation validation

For each of the somatic mutations identified by Exome-seq, we extracted the aligned mRNA-seq reads at its corresponding locus and examined if the mutant allele was also present in the cDNA sequences. The substitutions were called using SAMtools (Li et al. 2009). The small indels were called by both the SAMtools and Pindel algorithms (Ye et al. 2009). We focus on those loci covered by at least five reads, since it is rather difficult to call the variant accurately for poorly expressed genes. The mutation is supposed to be verified by mRNA-seq if at least two reads carried the mutant allele, and the mutant allele was detected in no less than 5% of the total reads aligned. For those loci covered by less than five reads but two or more reads, the mutation was also supposed to be verified if at least two reads carried the mutant allele.

Genome-wide SNP genotyping and DNA copy-number analysis

Genome-wide SNP genotyping was performed using the Affymetrix Genome-wide Human SNP Array 6.0 (Affymetrix) according to the manufacturer's instructions. SNPs were genotyped using the Birdseed version 2 module of the Affymetrix Genotyping Console software GTC 4.0.1, together with data from 45 HapMap-JPT samples (CEL files obtained from Affymetrix). DNA copy-number changes were analyzed using the Genome Imbalance Map (GIM) algorithm, as we previously described (Ishikawa et al. 2005).

The conventional MSI assay

The conventional MSI assay was performed using the proposed "Bethesda" panel of fluorescence-labeled markers, including *BAT25*, *BAT26*, *D2S123*, *D5S346*, and *D17S250* and an additional two markers, *NR21* and *NR27*. The primer sequences and PCR conditions have been previously described (Murayama-Hosokawa et al. 2010). In this study, we selected an additional three coding microsatellites and designed 6-carboxyfluorescein–labeled primers. Sequences of oligonucleotide primers for these three microsatellites are listed in Supplemental Table S4. PCR reactions were performed using the previously described reagents (Murayama-Hosokawa et al. 2010) under the following thermal cycle conditions: initial denature for 2 min at 94°C, followed by 32 cycles of denature for 15 sec at 94°C, annealing for 30 sec at 58°C, and primer extension for 30 sec at 68°C; the final extension step was carried out for 2 min at 68°C. After PCR, 1 μL of the properly diluted PCR product was mixed with 10 μL of Hi-Di Formamide and GeneScan 500 LIZ Size Standard (Applied Biosystems) mixture (37:1). This product was then denatured for 5 min at 95°C and put on ice immediately for 5 min before loading onto ABI 3130xl Genetic Analyzer (Applied Biosystems). The output data files were analyzed by GeneMapper Software Version 4.0 (Applied Biosystems). Determination of MSI status was made according to the presence of mutant alleles in tumor DNA compared with matched normal DNA.

MSI analysis by Exome-seq

We established a data analysis pipeline to identify small indels in the microsatellites. For each of the somatic indels identified in this study, we extracted the 50 bases of DNA sequences flanking its locus and examined if the indel was present in microsatellite sequences. Only those indels detected in the protein-coding microsatellites with at most 6 nt and repeated at least five times for mono- and dinucleotide microsatellites and at least three times for multiple-nucleotide microsatellites were counted. As shown in Figure 4, a graph was plotted for the indels in coding microsatellites according to the lengths of the indels and the number of sequence reads that supported the mutant alleles or the wild-type alleles. The microsatellite was suggested to be instable if a shorter allele (deletion) or a longer allele (insertion) was detected only in the tumor DNA. The sequence homology of each supporting read was further examined by the BLAT algorithm, and the reads rich of homologous sequences were discarded. The mutant allele ratio was then calculated using a formula as mentioned above.

MLH1 promoter methylation analysis

The methylation status of *MLH1* promoter was quantitatively measured using MassARRAY (Sequenom), as previously described (Yagi et al. 2010). Briefly, 500 ng gDNA was bisulfite converted using an EZ DNA Methylation Kit (Zymo Research) according to the manufacturer's instruction manual. Bisulfite-treated DNA was PCR amplified, and the PCR product was transcribed by in vitro transcription (IVT) prior to cleavage using RNase A. Unmethylated cytosine was converted to uracil by bisulfite treatment, while the methylated cytosine was not converted. Methylation status was then determined by the mass difference between A and G in the cleaved RNA product. Quantitative methylation scores were obtained at each analytic unit of a cleaved product, referred to as "CpG unit." The amplified DNA that was not methylated at all in any CpG sites was used as an unmethylated (0%) control. The amplified DNA, methylated by SssI methylase, was used as a fully methylated (100%) control.

Sanger sequencing

Oligo primers were designed to amplify the genome fragments containing the candidate nucleotide mutations from tumor cell line DNA and the matched normal DNA. PCR was performed using the high-fidelity DNA polymerase KOD-plus (TOYOBO) under optimized thermal conditions. PCR products were evaluated on a 2% agarose gel, purified and sequenced in both directions using Big Dye Terminator reactions, and subsequently loaded on an ABI 3130xl capillary sequencer (Applied Biosystems).

Statistical analysis

The *P*-value was calculated by Student's *t*-test when the data were normally distributed or by the nonparametric Wilcoxon signed-rank test when the data were not normally distributed. *P*-values less than 0.05 were considered to be statistically significant.

Data access

The Exome-seq data, mRNA-seq data, and SNP array data have been submitted to the European Genome-Phenome Archive (EGA; http://www.ebi.ac.uk/ega/), which is hosted at the European Bioinformatics Institute (EBI), under accession no. EGAS00001000149.

Acknowledgments

We thank Dr. Teruhiko Yoshida for having organized collaboration on the Exome-seq of the RCC project. We thank Ms. Kaori Shiina, Ms. Hiroko Meguro, Ms. Kaoru Nakano, and Ms. Saori Kawanabe for their excellent technical assistance. We acknowledge Dr. Michael Jones for the critical reading of the manuscript. This study was supported by Grants-in-Aid for Scientific Research (H.A.) and Scien-

tific Research on Priority Areas (H.A., T.N.); a grant for Translational Systems Biology and Medicine Initiative (TSBMI; H.A.) from the Ministry of Education, Culture, Sports, Science and Technology; the NFAT project from the New Energy and Industrial Technology Development Organization (NEDO; H.A., T.N.), Japan; and the Program for Promotion of Fundamental Studies in Health Sciences of the National Institute of Biomedical Innovation (NIBIO; T.S., H.S., Y.K.).

References

Arnold S, Buchanan DD, Barker M, Jaskowski L, Walsh MD, Birney G, Woods MO, Hopper JL, Jenkins MA, Brown MA, et al. 2009. Classifying MLH1 and MSH2 variants using bioinformatic prediction, splicing assays, segregation, and tumor characteristics. *Hum Mutat* **30:** 757–770.

Biesecker LG, Shianna KV, Mullikin JC. 2011. Exome sequencing: the expert view. *Genome Biol* **12:** 128. doi: 10.1186/gb-2011-12-9-128.

Bodmer W, Bielas JH, Beckman RA. 2008. Genetic instability is not a requirement for tumor development. *Cancer Res* **68:** 3558–3560.

Boland CR, Thibodeau SN, Hamilton SR, Sidransky D, Eshleman JR, Burt RW, Meltzer SJ, Rodriguez-Bigas MA, Fodde R, Ranzani GN, et al. 1998. A National Cancer Institute Workshop on Microsatellite Instability for cancer detection and familial predisposition: development of international criteria for the determination of microsatellite instability in colorectal cancer. *Cancer Res* **58:** 5248–5257.

Bronner CE, Baker SM, Morrison PT, Warren G, Smith LG, Lescoe MK, Kane M, Earabino C, Lipford J, Lindblom A, et al. 1994. Mutation in the DNA mismatch repair gene homologue hMLH1 is associated with hereditary non-polyposis colon cancer. *Nature* **368:** 258–261.

Choi M, Scholl UI, Ji W, Liu T, Tikhonova IR, Zumbo P, Nayir A, Bakkaloglu A, Ozen S, Sanjad S, et al. 2009. Genetic diagnosis by whole exome capture and massively parallel DNA sequencing. *Proc Natl Acad Sci* **106:** 19096–19101.

Cirulli ET, Singh A, Shianna KV, Ge D, Smith JP, Maia JM, Heinzen EL, Goedert JJ, Goldstein DB. 2010. Screening the human exome: a comparison of whole genome and whole transcriptome sequencing. *Genome Biol* **11:** R57. doi: 10.1186/gb-2010-11-5-r57.

Cunningham JM, Christensen ER, Tester DJ, Kim CY, Roche PC, Burgart LJ, Thibodeau SN. 1998. Hypermethylation of the hMLH1 promoter in colon cancer with microsatellite instability. *Cancer Res* **58:** 3455–3460.

Edelmann W, Cohen PE, Kane M, Lau K, Morrow B, Bennett S, Umar A, Kunkel T, Cattoretti G, Chaganti R, et al. 1996. Meiotic pachytene arrest in MLH1-deficient mice. *Cell* **85:** 1125–1134.

Fishel R, Lescoe MK, Rao MR, Copeland NG, Jenkins NA, Garber J, Kane M, Kolodner R. 1993. The human mutator gene homolog MSH2 and its association with hereditary nonpolyposis colon cancer. *Cell* **75:** 1027–1038.

Fujii K, Miyashita K, Yamada Y, Eguchi T, Taguchi K, Oda Y, Oda S, Yoshida MA, Tanaka M, Tsuneyoshi M. 2009. Simulation-based analyses reveal stable microsatellite sequences in human pancreatic cancer. *Cancer Genet Cytogenet* **189:** 5–14.

Greenman C, Stephens P, Smith R, Dalgliesh GL, Hunter C, Bignell G, Davies H, Teague J, Butler A, Stevens C, et al. 2007. Patterns of somatic mutation in human cancer genomes. *Nature* **446:** 153–158.

Harada T, Chelala C, Bhakta V, Chaplin T, Caulee K, Baril P, Young BD, Lemoine NR. 2008. Genome-wide DNA copy number analysis in pancreatic cancer using high-density single nucleotide polymorphism arrays. *Oncogene* **27:** 1951–1960.

Hatch SB, Lightfoot HM Jr, Garwacki CP, Moore DT, Calvo BF, Woosley JT, Sciarrotta J, Funkhouser WK, Farber RA. 2005. Microsatellite instability testing in colorectal carcinoma: choice of markers affects sensitivity of detection of mismatch repair-deficient tumors. *Clin Cancer Res* **11:** 2180–2187.

Hemminki A, Peltomaki P, Mecklin JP, Jarvinen H, Salovaara R, Nystrom-Lahti M, de la Chapelle A, Aaltonen LA. 1994. Loss of the wild type MLH1 gene is a feature of hereditary nonpolyposis colorectal cancer. *Nat Genet* **8:** 405–410.

Holbrook JA, Neu-Yilik G, Hentze MW, Kulozik AE. 2004. Nonsense-mediated decay approaches the clinic. *Nat Genet* **36:** 801–808.

Ishikawa S, Komura D, Tsuji S, Nishimura K, Yamamoto S, Panda B, Huang J, Fukayama M, Jones KW, Aburatani H. 2005. Allelic dosage analysis with genotyping microarrays. *Biochem Biophys Res Commun* **333:** 1309–1314.

Issaq SH, Lim KH, Counter CM. 2010. Sec5 and Exo84 foster oncogenic ras-mediated tumorigenesis. *Mol Cancer Res* **8:** 223–231.

Jiricny J. 1998. Eukaryotic mismatch repair: an update. *Mutat Res* **409:** 107–121.

Jones S, Zhang X, Parsons DW, Lin JC, Leary RJ, Angenendt P, Mankoo P, Carter H, Kamiyama H, Jimeno A, et al. 2008. Core signaling pathways in human pancreatic cancers revealed by global genomic analyses. *Science* **321:** 1801–1806.

Kim MP, Fleming JB, Wang H, Abbruzzese JL, Choi W, Kopetz S, McConkey DJ, Evans DB, Gallick GE. 2011. ALDH activity selectively defines an enhanced tumor-initiating cell population relative to CD133 expression in human pancreatic adenocarcinoma. *PLoS ONE* **6:** e20636. doi: 10.1371/journal.pone.0020636.

Kolodner RD, Marsischky GT. 1999. Eukaryotic DNA mismatch repair. *Curr Opin Genet Dev* **9:** 89–96.

Kuismanen SA, Holmberg MT, Salovaara R, de la Chapelle A, Peltomaki P. 2000. Genetic and epigenetic modification of MLH1 accounts for a major share of microsatellite-unstable colorectal cancers. *Am J Pathol* **156:** 1773–1779.

Kumar P, Henikoff S, Ng PC. 2009. Predicting the effects of coding non-synonymous variants on protein function using the SIFT algorithm. *Nat Protoc* **4:** 1073–1081.

Lengauer C, Kinzler KW, Vogelstein B. 1998. Genetic instabilities in human cancers. *Nature* **396:** 643–649.

Li H, Durbin R. 2009. Fast and accurate short read alignment with Burrows-Wheeler transform. *Bioinformatics* **25:** 1754–1760.

Li H, Handsaker B, Wysoker A, Fennell T, Ruan J, Homer N, Marth G, Abecasis G, Durbin R. 2009. The Sequence Alignment/Map format and SAMtools. *Bioinformatics* **25:** 2078–2079.

Li Y, Vinckenbosch N, Tian G, Huerta-Sanchez E, Jiang T, Jiang H, Albrechtsen A, Andersen G, Cao H, Korneliussen T, et al. 2010. Resequencing of 200 human exomes identifies an excess of low-frequency non-synonymous coding variants. *Nat Genet* **42:** 969–972.

Ma S, Chan YP, Woolcock B, Hu L, Wong KY, Ling MT, Bainbridge T, Webber D, Chan TH, Guan XY, et al. 2009. DNA fingerprinting tags novel altered chromosomal regions and identifies the involvement of SOX5 in the progression of prostate cancer. *Int J Cancer* **124:** 2323–2332.

Maitra A, Hruban RH. 2008. Pancreatic cancer. *Annu Rev Pathol* **3:** 157–188.

Marra G, Schar P. 1999. Recognition of DNA alterations by the mismatch repair system. *Biochem J* **338:** 1–13.

Metzker ML. 2010. Sequencing technologies—the next generation. *Nat Rev Genet* **11:** 31–46.

Murayama-Hosokawa S, Oda K, Nakagawa S, Ishikawa S, Yamamoto S, Shoji K, Ikeda Y, Uehara Y, Fukayama M, McCormick F, et al. 2010. Genome-wide single-nucleotide polymorphism arrays in endometrial carcinomas associate extensive chromosomal instability with poor prognosis and unveil frequent chromosomal imbalances involved in the PI3-kinase pathway. *Oncogene* **29:** 1897–1908.

Nakahori S, Yokosuka O, Ehata T, Chuang WL, Imazeki F, Ito Y, Ohto M. 1995. Detection of hepatitis B virus precore stop codon mutants by selective amplification method: frequent detection of precore mutants in hepatitis B e antigen positive healthy carriers. *J Gastroenterol Hepatol* **10:** 419–425.

Negrini S, Gorgoulis VG, Halazonetis TD. 2010. Genomic instability: an evolving hallmark of cancer. *Nat Rev Mol Cell Biol* **11:** 220–228.

Ng SB, Turner EH, Robertson PD, Flygare SD, Bigham AW, Lee C, Shaffer T, Wong M, Bhattacharjee A, Eichler EE, et al. 2009. Targeted capture and massively parallel sequencing of 12 human exomes. *Nature* **461:** 272–276.

Ng SB, Buckingham KJ, Lee C, Bigham AW, Tabor HK, Dent KM, Huff CD, Shannon PT, Jabs EW, Nickerson DA, et al. 2010. Exome sequencing identifies the cause of a mendelian disorder. *Nat Genet* **42:** 30–35.

Parsons DW, Jones S, Zhang X, Lin JC, Leary RJ, Angenendt P, Mankoo P, Carter H, Siu IM, Gallia GL, et al. 2008. An integrated genomic analysis of human glioblastoma multiforme. *Science* **321:** 1807–1812.

Qiu W, Tong GX, Manolidis S, Close LG, Assaad AM, Su GH. 2008. Novel mutant-enriched sequencing identified high frequency of PIK3CA mutations in pharyngeal cancer. *Int J Cancer* **122:** 1189–1194.

Raschle M, Marra G, Nystrom-Lahti M, Schar P, Jiricny J. 1999. Identification of hMutLβ, a heterodimer of hMLH1 and hPMS1. *J Biol Chem* **274:** 32368–32375.

Schuster SC. 2008. Next-generation sequencing transforms today's biology. *Nat Methods* **5:** 16–18.

Shibata T, Saito S, Kokubu A, Suzuki T, Yamamoto M, Hirohashi S. 2010. Global downstream pathway analysis reveals a dependence of oncogenic NF-E2–related factor 2 mutation on the mTOR growth signaling pathway. *Cancer Res* **70:** 9095–9105.

Sjoblom T, Jones S, Wood LD, Parsons DW, Lin J, Barber TD, Mandelker D, Leary RJ, Ptak J, Silliman N, et al. 2006. The consensus coding sequences of human breast and colorectal cancers. *Science* **314:** 268–274.

Stratton MR, Campbell PJ, Futreal PA. 2009. The cancer genome. *Nature* **458:** 719–724.

Sugarbaker DJ, Richards WG, Gordon GJ, Dong L, De Rienzo A, Maulik G, Glickman JN, Chirieac LR, Hartman ML, Taillon BE, et al. 2008.

Transcriptome sequencing of malignant pleural mesothelioma tumors. *Proc Natl Acad Sci* **105:** 3521–3526.
Suter CM, Martin DI, Ward RL. 2004. Germline epimutation of MLH1 in individuals with multiple cancers. *Nat Genet* **36:** 497–501.
Thomas RK, Nickerson E, Simons JF, Janne PA, Tengs T, Yuza Y, Garraway LA, LaFramboise T, Lee JC, Shah K, et al. 2006. Sensitive mutation detection in heterogeneous cancer specimens by massively parallel picoliter reactor sequencing. *Nat Med* **12:** 852–855.
Toma MI, Grosser M, Herr A, Aust DE, Meye A, Hoefling C, Fuessel S, Wuttig D, Wirth MP, Baretton GB. 2008. Loss of heterozygosity and copy number abnormality in clear cell renal cell carcinoma discovered by high-density affymetrix 10K single nucleotide polymorphism mapping array. *Neoplasia* **10:** 634–642.
Totoki Y, Tatsuno K, Yamamoto S, Arai Y, Hosoda F, Ishikawa S, Tsutsumi S, Sonoda K, Totsuka H, Shirakihara T, et al. 2011. High-resolution characterization of a hepatocellular carcinoma genome. *Nat Genet* **43:** 464–469.
Trapnell C, Pachter L, Salzberg SL. 2009. TopHat: discovering splice junctions with RNA-Seq. *Bioinformatics* **25:** 1105–1111.
Varela I, Tarpey P, Raine K, Huang D, Ong CK, Stephens P, Davies H, Jones D, Lin ML, Teague J, et al. 2011. Exome sequencing identifies frequent mutation of the SWI/SNF complex gene PBRM1 in renal carcinoma. *Nature* **469:** 539–542.
Vogelstein B, Kinzler KW. 2004. Cancer genes and the pathways they control. *Nat Med* **10:** 789–799.
Wilentz RE, Goggins M, Redston M, Marcus VA, Adsay NV, Sohn TA, Kadkol SS, Yeo CJ, Choti M, Zahurak M, et al. 2000. Genetic, immunohistochemical, and clinical features of medullary carcinoma of the pancreas: A newly described and characterized entity. *Am J Pathol* **156:** 1641–1651.
Wood LD, Parsons DW, Jones S, Lin J, Sjoblom T, Leary RJ, Shen D, Boca SM, Barber T, Ptak J, et al. 2007. The genomic landscapes of human breast and colorectal cancers. *Science* **318:** 1108–1113.
Yagi K, Akagi K, Hayashi H, Nagae G, Tsuji S, Isagawa T, Midorikawa Y, Nishimura Y, Sakamoto H, Seto Y et al. 2010. Three DNA methylation epigenotypes in human colorectal cancer. *Clin Cancer Res* **16:** 21–33.
Yamano M, Fujii H, Takagaki T, Kadowaki N, Watanabe H, Shirai T. 2000. Genetic progression and divergence in pancreatic carcinoma. *Am J Pathol* **156:** 2123–2133.
Ye K, Schulz MH, Long Q, Apweiler R, Ning Z. 2009. Pindel: a pattern growth approach to detect break points of large deletions and medium sized insertions from paired-end short reads. *Bioinformatics* **25:** 2865–2871.

Received March 9, 2011; accepted in revised form October 3, 2011.

The Carcinoembryonic Antigen Level in Pancreatic Juice and Mural Nodule Size Are Predictors of Malignancy for Branch Duct Type Intraductal Papillary Mucinous Neoplasms of the Pancreas

Seiko Hirono, MD, Masaji Tani, MD, Manabu Kawai, MD, Ken-ichi Okada, MD, Motoki Miyazawa, MD, Atsushi Shimizu, MD, Yuji Kitahata, MD, and Hiroki Yamaue, MD

Objective: Identification of predictors of malignancy for branch duct type intraductal papillary mucinous neoplasms (IPMN).

Background: Main duct type IPMN has been recommended for resection. However, the indications for resection of the branch duct type IPMN have been controversial.

Methods: We retrospectively analyzed the clinicopathological factors of 134 patients undergoing resection for branch duct type IPMN, excluding main duct type IPMN, to identify predictors of the malignant behavior of this neoplasm. The cutoff values of tumor size, main pancreatic duct (MPD) size, mural nodule size, and carcinoembryonic antigen (CEA) level in the pancreatic juice obtained during preoperative endoscopic retrograde pancreatography (ERP) were analyzed using receiver–operator characteristic curves.

Results: We found 7 significant predictors for malignancy in the branch duct type IPMN in a univariate analysis; jaundice, tumor occupying the pancreatic head, MPD size >5 mm, mural nodule size >5 mm, serum carbohydrate antigen (CA)19–9 level, positive cytology in the pancreatic juice, and CEA level in the pancreatic juice >30 ng/mL. In a multivariate analysis, a mural nodule size >5 mm and a CEA level in the pancreatic juice >30 ng/mL were independent factors associated with malignancy. The positive predictive value of a mural nodule size >5 mm and a CEA level in the pancreatic juice >30 ng/mL was 100%, and the negative predictive value was 96.3%.

Conclusions: We identified 2 useful predictive factors for malignancy in branch duct type IPMN; a mural nodule size >5 mm and a CEA level in the pancreatic juice obtained by preoperative ERP >30 ng/mL.

(*Ann Surg* 2012;255:517–522)

As a result of improvements of radiological imaging and increased clinician awareness, intraductal papillary mucinous neoplasm (IPMN) of the pancreas has been recognized with increasing frequency because it was formally defined in 1996 by the World Health Organization.[1] It has been established that IPMN has malignant potential and that it first transforms from an adenoma to a borderline neoplasm, then develops into carcinoma, including carcinoma in situ (CIS), and ultimately becomes an invasive carcinoma [invasive IPMC (intraductal papillary mucinous carcinoma)].[1] In general, IPMN has a favorable prognosis, because of its indolent biological behavior; therefore, excellent survival outcomes have been reported after complete resection in the patients with noninvasive IPMN, including adenoma, borderline neoplasm, and CIS.[2–6] However, once IPMN progresses to invasive carcinoma, it becomes aggressive and is associated with a poor prognosis, with the 5-year survival in patients with invasive IPMC reportedly ranging from 22% to 67%.[7–9] Therefore, the timing of resection is important for the successful treatment of IPMN, and it is necessary to establish a treatment protocol and surgical indications for patients with IPMN.

Depending on the morphology of the changes of the ductal system, IPMNs have been classified into the 3 variations—main duct type, branch duct type, and mixed type by radiological imaging. Many recent clinicopathological studies have shown that IPMNs arising in the main pancreatic duct (MPD) are more aggressive than those arising in the branch pancreatic duct (BPD), and the malignancy rate of main duct type IPMN has been reported to be 57% to 92%,[4–6,10] whereas that of branch duct type IPMN has been reported to be 6% to 58%.[10–14] Therefore, although most clinicians agree that surgical resection is required for all main duct type IPMNs, the management of branch duct type IPMNs remains controversial, because branch duct type IPMN generally has a low risk of malignancy.

We previously suggested that measurement of the carcinoembryonic antigen (CEA) level in the pancreatic juice obtained during preoperative endoscopic retrograde pancreatography (ERP) was useful for distinguishing malignant from benign IPMNs,[2,3]; however, our previous studies had 2 problems: (1) a small number of patients analyzed (n = 54), and (2) the subjects in the study were patients with all types of IPMNs, including the main duct type. Therefore, in the present study, we examined 134 patients with IPMNs, other than the main duct type, and reanalyzed the cutoff values for predicting malignancy of the tumor size, MPD size, mural nodule size, and the CEA level in the pancreatic juice, using receiver–operator characteristic (ROC) curves. We retrospectively analyzed the clinical and imaging findings and laboratory data to identify the predictors of malignancy and determined the optimal indications for the patients with branch duct type IPMN.

MATERIALS AND METHODS

Patient Enrollment

From July 1999 to February 2011, 196 consecutive patients with IPMN underwent a pancreatectomy at Wakayama Medical University Hospital. We classified the patients into 2 groups on the basis of their type of IPMN as determined by preoperative imaging studies; main duct type IPMN and branch duct type IPMN. We defined the main duct type IPMN as that found to have diffuse or segmental MPD dilation, but not cyst formation caused by BPD dilation. Next, we defined the branch duct type IPMN as that with cyst formation caused by BPD dilation with or without MPD dilation. In this study, we excluded 23 patients who had IPMN concomitant with common pancreatic cancer. Among the remaining 173 consecutive patients with resected IPMNs, 134 patients were classified as having branch duct type IPMN, and all were enrolled in this study. The study protocol was approved by the Human Ethics Review Committee of Wakayama Medical University Hospital, and a signed consent form was obtained from each subject.

From the Second Department of Surgery, Wakayama Medical University, School of Medicine, Kimiidera, Wakayama, Japan.

Disclosure: The authors declare that they have nothing to disclose.

Reprints: Hiroki Yamaue, MD, Second Department of Surgery, Wakayama Medical, University, School of Medicine, 811–1 Kimiidera, Wakayama 641–8510, Japan. E-mail: yamaue-h@wakayama-med.ac.jp.

ISSN: 0003-4932/12/25503-0517
DOI: 10.1097/SLA.0b013e3182444231

Preoperative Examination and Indications for Surgery

Before surgery, all patients underwent a clinical evaluation, routine laboratory tests including the assessment of tumor markers, abdominal ultrasonography (US), and computed tomography (CT). Magnetic resonance imaging cholangiopancreatography and endoscopic US (EUS) were performed in 131 and 125 patients, respectively. Endoscopic retrograde pancreatography was performed in all patients with branch duct type IPMN, excluding the 4 patients undergoing Billroth II reconstruction after distal gastrectomy. Preoperative pancreatic juice cytology (n = 104) and measurement of CEA levels in pancreatic juice (n = 91) were performed using the samples obtained during preoperative ERP, using the previously reported method.[2,3] Briefly, the pancreatic juice in the MPD was collected by preoperative ERP, and immediately centrifuged, and the precipitate was used for cytological examination, and the CEA levels in the supernatant were measured by means of a CEA immunometric chemiluminescent assay kit (Bayer Medical Co, Tokyo, Japan). The tumor size was measured by CT, and the mural nodule size was determined by EUS in 125 patients who underwent preoperative EUS, and by CT in other 9 patients without performing EUS.

Surgery was performed in the patients with IPMN who met at least one of the following criteria: (1) the presence of symptoms, (2) main duct type IPMN, (3) the presence of mural nodules, (4) an MPD larger than 7 mm in diameter, or gradual dilation of the MPD observed during follow-up, (5) tumor size larger than 30 mm, or a gradual increase in the tumor size during follow-up, (6) class IV or V in cytology of the pancreatic juice, or (7) a CEA level higher than 110 ng/mL in the pancreatic juice, which was the cutoff level identified by analyzing the difference between benign and malignant IPMNs in all patients with all types of IPMN, using ROC curves, as previously reported.[2,3]

All resected specimens were examined pathologically and classified into adenoma, borderline, CIS, and invasive IPMC, according to the classification established by the World Health Organization by 2 independent pathologists (A.Y. and Y.N.). *Invasive IPMC* was defined as that presenting the pathological findings of continuance of an invasive component from CIS, to distinguish it from common pancreatic ductal cancer concomitant with IPMN.

Statistical Analysis

For the purpose of the analyses, we classified IPMN with adenoma and borderline neoplasm as a benign IPMN group, whereas CIS and invasive IPMC were classified as a malignant IPMN group. The cutoff levels for the tumor size, MPD size, mural nodule size, and CEA level in the pancreatic juice were determined to maximize the difference between benign and malignant IPMNs by ROC curves (SPSS, Release 17.0; SPSS Inc, Chicago, IL). The 16 preoperative potential risk factors were assessed by a univariate analysis with the χ^2 and included the patient age, sex, symptoms, jaundice, body weight loss, abdominal pain, back pain, diabetes mellitus, the tumor location, tumor size, MPD size, mural nodule size, serum CEA level, serum carbohydrate antigen (CA) 19–9 level, cytology in the pancreatic juice, and CEA levels in the pancreatic juice (SPSS, Release 17.0). The $P < 0.1$ predictors of malignant IPMN in the univariate analysis were then included in a forward stepwise multiple logistic regression model (SPSS, Release 17.0). Statistical significance was defined as $P < 0.05$.

RESULTS

Patient Characteristics and Histopathological Findings

Table 1 shows the characteristics of the enrolled patients. This study included 74 men and 60 women, with a mean age ± standard deviation of 68.9 ± 9.7 years. The mean tumor size, mean MPD size, and the mean mural nodule size were 30.4 ± 12.3, 6.5 ± 4.2, and 5.5 ± 5.0, respectively. A total pancreatectomy was performed in 3 patients (2.2%); a pancreatoduodenectomy (PD), including a pylorus-preserving PD and a pylorus-resecting PD, was performed in 101 patients (75.4%); a distal pancreatectomy was performed in 14 patients (10.5%); and a central pancreatectomy was performed in 16 patients (11.9%). Combined venous resection (portal vein or superior mesenteric vein) was performed in 10 patients (7.4%), and combined celiac artery resection was performed in 1 patient (0.8%).

In the 134 patients with branch duct type IPMN, there were 56 patients (41.8%) with benign IPMN, including 51 with adenomas and 5 with borderline neoplasms, and there were 41 patients (30.6%) with CIS, and 37 patients (27.6%) with invasive IPMC, including 5 with minimally invasive IPMC (Table 1).

Complications of ERP and Pancreatic Duct Irrigation

The definition of post-ERP acute pancreatitis and the grading of its severity were based on consensus criteria.[15] Seven patients (5.4%) developed pancreatitis in 130 patients who underwent preoperative ERP. Among them, 5 patients (4.8%) developed pancreatitis (moderate in 1 patient and mild in 4 patients) in 104 patients whose pancreatic juice obtained by ERP.

Diagnostic Cutoff Levels for the Tumor Size, MPD Size, Mural Nodule Size, and CEA Levels in the Pancreatic Juice for the Prediction of Malignant IPMN

In this study, ROC curves were used to determine the cutoff levels for the tumor size, MPD size, mural nodule size, and CEA level in the pancreatic juice (Fig. 1) to differentiate between benign and malignant IPMN in the patients with the branch duct type IPMN. Mathematically, the cutoff values were defined as those corresponding to points on the ROC curve situated furthest away from the reference line. The areas under curve for the tumor size, MPD size, mural nodule size, and CEA level in the pancreatic juice were 0.612, 0.711, 0.819, and 0.920, respectively, and the determined cutoff levels for the differentiation between benign and malignant IPMNs were 30 mm, 5 mm, 5 mm, and 30 ng/mL, respectively (Table 2).

TABLE 1. The Demographics and Clinical Characteristics of 134 Patients With Branch Duct Type IPMN

Characteristics	Value
Age, mean ± SD (range), yr	68.9 ± 9.7 (32–84)
Sex, male/female	74/60
Tumor size, mean ± SD (range), mm	30.4 ± 12.3 (5–88)
Main pancreatic duct size, mean ± SD (range), mm	6.5 ± 4.2 (1–20)
Mural nodule size, mean ± SD (range), mm	5.5 ± 5.0 (0–20)
Operation	
Total pancreatectomy	3 (2.2%)
Pancreatoduodenectomy (PD/PpPD/PrPD)	101(17/43/41) (75.4%)
Distal pancreatectomy	14 (10.5%)
Central pancreatectomy	16 (11.9%)
Histopathology	
Adenoma	51 (38.1%)
Borderline	5 (3.7%)
Carcinoma in situ	41 (30.6%)
Invasive IPMC	37 (27.6%)

PpPD indicates pylorus-preserving PD; PrPD, pylorus-resecting PD

Predictors of Malignancy for Branch Duct Type IPMN

In the univariate analysis, we found 7 significant factors predicting the malignancy of branch duct type IPMNs: the presence of jaundice ($P < 0.001$), a tumor occupying the pancreatic head ($P = 0.006$), a MPD size larger than 5 mm ($P < 0.001$), mural nodule size larger than 5 mm ($P < 0.001$), elevated serum CA19–9 ($P = 0.002$), positive cytology (class IV or V) in the pancreatic juice ($P = 0.023$), and a CEA level in the pancreatic juice >30 ng/mL ($P < 0.001$) (Table 3). Furthermore, a mural nodule size larger than 5 mm ($P = 0.003$; odds ratio = 12.9) and a CEA level in the pancreatic juice higher than 30 ng/mL ($P < 0.001$; odds ratio = 299) were independent malignant predictors in the subsequent multivariate analysis (Table 4).

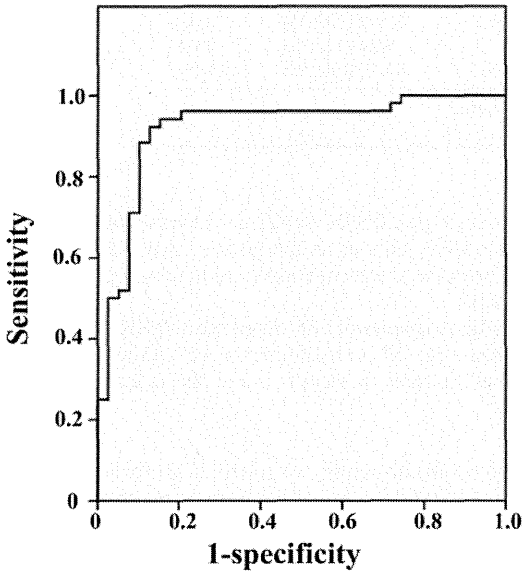

FIGURE 1. The receiver operating characteristic curve used to determine the optimal CEA cutoff levels in the pancreatic juice obtained by preoperative endoscopic retrograde pancreatography for the prediction of the malignancy of branch duct type IPMN. The area under the curve for the CEA levels in the pancreatic juice was 0.92, and the determined cutoff level for differentiation between benign and malignant IPMNs was 30 ng/mL.

TABLE 2. The Diagnostic Cutoff Levels of the Tumor Size, Main Duct Size, Mural Nodule Size, and CEA Levels in the Pancreatic Juice for Differentiating Between Benign and Malignant IPMN Based on the Receiver Operating Characteristic Curves

	Area Under Curve	Cutoff Value
Tumor size	0.612	30 mm
Main pancreatic duct size	0.711	5 mm
Mural nodule size	0.819	5 mm
CEA levels in the pancreatic juice*	0.920	30 ng/mL

*The CEA in the pancreatic juice could be measured in 91 patients who received preoperative ERP.

With regard to the mural nodule size, the sensitivity, specificity, and accuracy of the cutoff (5 mm) for differentiating between benign and malignant IPMN were 74.4%, 80.4%, and 76.9%, respectively and those for the CEA cutoff level in the pancreatic juice (30 ng/mL) were 94.2%, 84.6%, and 90.1%, respectively.

We found that mural nodule size determined by EUS and CEA levels in the pancreatic juice were significantly correlated ($P < 0.001$; Table 5). There were 5 patients with just 5 mm of mural nodule with a CEA level in the pancreatic juice higher than 30 ng/mL, and they included 4 patients with adenoma and 1 patient with CIS.

Combination Analysis of the Mural Nodule Size and CEA Level in the Pancreatic Juice

If the analyses of the mural nodule size and CEA level in the pancreatic juice were combined, all patients with a mural nodule size larger than 5 mm who also had a CEA level in the pancreatic juice higher than 30 ng/mL had malignancy, indicating that the positive predictive value of both a mural nodule larger than 5 mm and a CEA level in the pancreatic juice higher than 30 ng/mL was 100%. Moreover, 26 patients of the 27 patients with a mural nodule size larger than 5 mm and a CEA level in the pancreatic juice higher than 30 ng/mL had benign IPMN, indicating that the negative predictive value of both a mural nodule size larger than 5 mm or a CEA level in the pancreatic juice higher than 30 ng/mL was 96.3% (Fig. 2).

DISCUSSION

Surgical resection offers the best chance for a cure for the patients with IPMN; however, observation may be a better management strategy for the patients with a low risk of malignancy, because a pancreatectomy is an invasive procedure, especially in elderly patients.[16] Therefore, many investigators have performed studies to identify factors that can be used to predict the likelihood of malignancy in the patients with IPMNs. Most clinicians have agreed that the main duct type IPMN has high malignant potential, and surgical resection is recommended for all patients with main duct type IPMN.[4–6,10] However, there is still no definite management consensus, including the surgical indications, for patients with branch duct type IPMN, because the malignant potential of branch duct type IPMN is relatively low.[10–14] Thus, it is necessary to identify more accurate factors that can predict the malignancy and determine the indications for surgical resection for the patients with the branch duct type IPMN.

The International Consensus Guidelines have put forward an algorithm for the surgical management of branch duct type IPMN, which is based on the tumor size, patient symptoms, and "high risk stigmata" (mural nodule and positive cytology in the pancreatic juice).[17] Several recent studies reported that the size of mural nodules was a more significant malignant factor than the tumor size for predicting the malignancy of branch duct type IPMN.[6,10,12,14] In addition, the MPD size, positive EUS fine-needle aspiration (FNA) cytology, and high CEA or carbohydrate antigen (CA)72.4 levels in the cystic fluid have been reported to be factors that can be used to predict the malignancy of branch duct type IPMN.[5,18–21] However, the accuracies of these factors were not high enough to distinguish between benign and malignant IPMNs. Moreover, the cytology of the pancreatic juice should be a criterion standard for the preoperative pathological diagnosis. However, the sensitivity of preoperative cytology was only 11.1% in this series. Therefore, we tried to identify more accurate predictors of the malignant potential of branch duct IPMN to determine an optimal management consensus. If CIS could be determined for the patients with branch duct type IPMN by several parameters, that would be powerful. However, in this study, the number of CIS was small; only 41 patients. Therefore, we could not analyze separately in each group. In the future, we would like to try

TABLE 3. The Results of the Univariate Analysis of the Malignant Predictive Factors for Branch Duct Type IPMN

	Benign (n = 56), n (%)	Malignant (n = 78), n (%)	*P*
Age, >70 yr	25/56 (44.6%)	44/78 (56.4%)	0.179
Sex, male	30/56 (53.6%)	44/78 (56.4%)	0.745
Symptom	27/56 (48.2%)	46/78 (59%)	0.217
Jaundice	0 (0%)	14 (18%)	<0.001
Body weight loss	5 (8.9%)	11 (14.1%)	0.362
Abdominal pain	14 (25%)	23 (29.5%)	0.567
Back pain	9 (16.1%)	9 (11.5%)	0.448
Onset or worsening of diabetes mellitus	13/56 (23.2%)	26/78 (33.3%)	0.203
Tumor occupied location, head	35/56 (62.5%)	65/78 (83.3%)	0.006
Tumor size, >30 mm	20/56 (35.7%)	37/78 (47.4%)	0.176
Main pancreatic duct size, >5 mm	16/56 (28.6%)	52/78 (66.7%)	<0.001
Mural nodule size, >5 mm	11/56 (19.6%)	57/78 (73.1%)	<0.001
Serum CEA, elevated	3/56 (5.4%)	9/78 (11.5%)	0.217
Serum CA19–9, elevated	6/56 (10.7%)	27/78 (34.6%)	0.002
Cytology in the pancreatic juice,* class IV or V	0/44 (0%)	6/54 (11.1%)	0.023
CEA levels in the pancreatic juice,† >30 ng/m	6/39 (15.4%)	49/52 (94.2%)	<0.001

*Cytological examination of the pancreatic juice was possible in 98 patients.
†The CEA in the pancreatic juice could be measured in 91 patients.

TABLE 4. The Results of the Multivariate Analysis of the Malignant Predictive Factors for Branch Duct Type IPMN

	P	Odds Ratio	95% Confidence Interval
Jaundice	0.989		
Tumor occupied location, head	0.136		
Main pancreatic duct size, >5 mm	0.082		
Mural nodule size, >5 mm	0.003	12.9	2.38–70.3
Serum CA19–9, elevated	0.803		
Cytology in the pancreatic, class IV or V	0.983		
CEA levels in the pancreatic juice, >30 ng/mL	<0.001	299	17.7–5067

TABLE 5. Correlation Between Findings of EUS and CEA in the Pancreatic Juice Obtained by ERP for the Patients With Branch Duct Type IPMN

EUS Findings (Mural Nodule Size)	CEA Levels in the Pancreatic Juice Obtained by ERP		
	≤30 ng/mL (n = 36)	>30 ng/mL (n = 55)	*P*
≤5 mm (n = 45)	27	18	<0.001
>5 mm (n = 46)	9	37	

to analyze by clustering the patients with branch duct type IPMN into 3 groups—adenoma, CIS, and invasive IPMC.

In this study, we defined branch duct type IPMN as that with cyst formation caused by BPD dilation with or without MPD dilation. The reasons that we included mixed type IPMN into the branch duct type IPMN are as follows:

1. It is difficult to distinguish branch duct type IPMN with MPD dilatation caused by outflow of copious mucin from a side branch cyst from the mixed type IPMN with MPD dilatation resulting from the production of mucin in the MPD,[6] by preoperative radiological imaging.
2. Branch duct type IPMN sometimes has microscopic involvement into the MPD without radiological evidence of dilatation of the MPD; however, the preoperative prediction of this phenomenon is impossible.
3. The malignant potential of mixed type IPMN was reported to be lower than that of the main duct type,[6] although there have been a limited number of reports about the potential of mixed type IPMN.

Indeed, in this study, we found 22 patients with branch duct IPMN with MPD dilation, ie, mixed type on imaging findings (the pathological diagnosis in branch pancreatic duct is 5 adenoma, 10 CIS, and 7 invasive IPMC). In 5 mixed type IPMN patients with adenoma, only 1 patient had an adenoma in MPD. Remaining 4 patients had no atypia in MPD, which had the secondary dilation of MPD because of inflow of mucinous fluid from cystic branch duct. Thus, it is very difficult to distinguish branch duct type IPMN from mixed type IPMN by radiological imaging, because we could not predict microscopic involvement into MPD in mixed type IPMN patients.

For this study, we reanalyzed the cutoff values for the tumor size, MPD size, mural nodule size, and CEA level in the pancreatic juice to distinguish between benign and malignant IPMN exclusively in patients with branch duct type IPMN, using ROC curves. Our results suggested that a mural nodule size larger than 5 mm and a CEA level in the pancreatic juice obtained by preoperative ERP higher than 30 ng/mL were independent significant predictors of malignancy in a multivariate analysis. In several significant malignant predictors for branch duct type IPMN on univariate analysis, but not significant on multivariate analysis, we found jaundice, MPD dilation, and elevated serum CA19–9 as malignant predictive factors for IPMN.[10–14] All 8 branch duct type IPMN patients with jaundice, MPD dilation, and elevated serum CA19–9 had malignancy, whereas in 32 patients without jaundice, MPD dilation or elevated serum CA19–9, 10 patients had malignancy with a high CEA in the pancreatic juice. Therefore, the branch duct type IPMN patients with jaundice, MPD dilation, and elevated serum CA19–9 may not require ERP, because the positive predictive values for malignancy of combination of these 3 factors are high, whereas ERP may be useful procedure to distinguish between

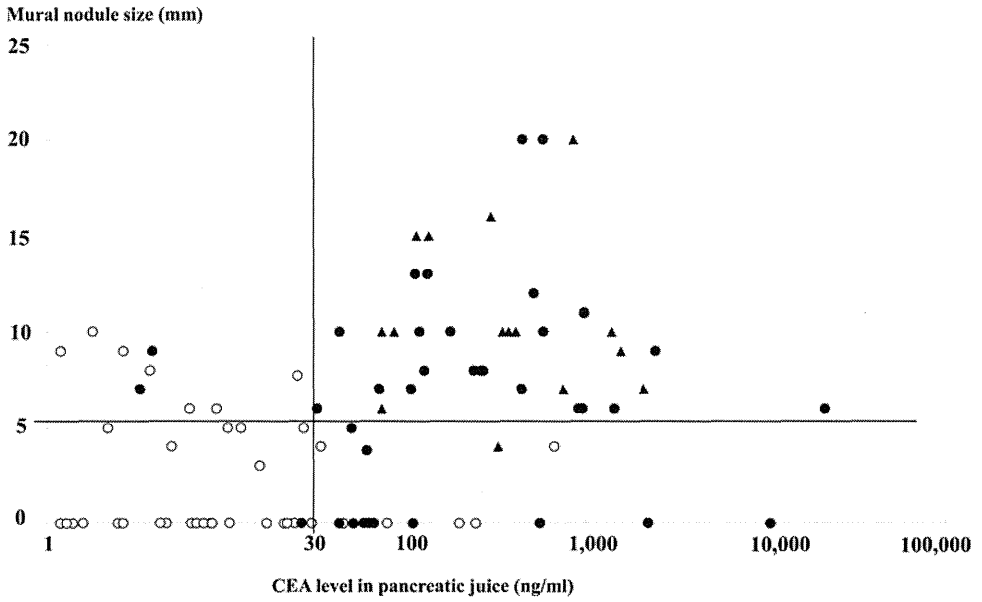

FIGURE 2. The distribution of the mural nodule size and CEA levels in the pancreatic juice in patients with branch duct type IPMN. IPMNs classified as adenoma and borderline neoplasm are indicated by white circles (○), carcinoma in situ by black circles (●), and invasive IPMC by black triangles (▲). All patients (100%) with a mural nodule size larger than 5 mm and a CEA level in the pancreatic juice higher than 30 ng/mL had malignant IPMN, whereas only 1 patient among 27 with a mural nodule size ≤5 mm and a CEA level in the pancreatic juice 30 ng/mL or lower had malignant IPMN.

benign and malignant IPMNs for patients without jaundice, MPD dilation, nor elevated serum CA19–9.

We previously reported that the cutoff value for the CEA level in the pancreatic juice to distinguish malignant from benign IPMN was 110 ng/mL for the patients with all types IPMN,[2] whereas this study suggested that the cutoff value was 30 ng/mL for the patients with branch duct type IPMN. It is considered that the CEA levels in main duct type IPMN are higher than those of other types of IPMN, because the CEA levels of the pancreatic juice obtained from the MPD reflect the direct secretion of CEA for the main duct type, whereas the CEA levels for the branch duct type IPMN reflect the outflow into the MPD from cystic side branch secretions.

Recently, measurements of CEA or/and CA72.4 in the cystic fluid obtained by EUS-FNA were reported to be useful for the differentiation of malignant from benign IPMN.[20] In our institute, we have measured the CEA levels in the pancreatic juice obtained from the MPD by preoperative ERP in the patients with all types IPMN, but not in the cyst fluid obtained by EUS-FNA, because (1) obtaining pancreatic juice by ERP is not associated with any risk of peritoneal seeding, and actually, peritoneal seeding was not found in all patients, whose pancreatic juice obtained by preoperative ERP, and (2) the branch duct type IPMNs are often consisted of multilocular cysts, and it is unknown which cyst has the most severe atypia, whereas the pancreatic juice in the MPD obtained by ERP includes secreted CEA from all of the pancreatic ducts. However, further studies of the evaluation of the correlations between the CEA levels in the pancreatic juice in the MPD and the CEA levels in the cyst fluid should be performed.

In this study, there were 29 patients with a mural nodule size 5 mm or smaller and a tumor size 30 mm or larger, who were predicted to have benign IPMN by findings of EUS and CT. Among 29 patients, we had 8 malignant IPMN patients with a CEA level in the pancreatic juice obtained by ERP more than 30 ng/mL. Furthermore, in 23 patients with branch duct type IPMN without a mural nodule and a tumor size 30 mm or smaller, 6 patients had malignancy with a CEA level in the pancreatic juice higher than 30 ng/mL. These results suggest that ERP may be a useful procedure for some branch duct type IPMN patients with a mural nodule size 5 mm or smaller and a tumor size 30 mm or smaller, whereas we cannot clarify which types of patients would be benefited from this additional invasive procedure.

When the combination of a mural nodule size larger than 5 mm and a CEA level in the pancreatic juice higher than 30 ng/mL is used, the predictive value is excellent (100%), indicating that branch duct type IPMN with a mural nodule size larger than 5 mm and a CEA level in the pancreatic juice higher than 30 ng/mL would be recommended for resection. Only 1 patient (1 of 27 patients) with a mural nodule size 5 mm or smaller and a CEA level in the pancreatic juice 30 ng/mL or lower had malignant IPMN, which suggests that the patients with branch duct type IPMN in this group might be better treated by strict observation.

In conclusion, we identified 2 useful predictive factors for malignancy in branch duct type IPMN; a mural nodule size larger than 5 mm and a CEA level in the pancreatic juice obtained by preoperative ERP more than 30 ng/mL. Additional studies in other populations will be needed to confirm the validity of our findings.

REFERENCES

1. Kloppel G, Solcia E, Longnecker DS, et al. *Histologic Typing of Tumors of the Exocrine Pancreas*. 2nd ed. Geneva, Switzerland: Springer-Verlag; 1996.
2. Kawai M, Uchiyama K, Tani M, et al. Clinicopathological features of malignant intraductal papillary mucinous tumors of the pancreas. *Arch Surg*. 2004;139:188–192.
3. Hirono S, Tani M, Kawai M, et al. Treatment strategy for intraductal papillary mucinous neoplasm of the pancreas based on malignant predictive factors. *Arch Surg*. 2009;144:345–349.
4. Jang JY, Hwang DW, Kim MA, et al. Analysis of prognostic factors and a proposed new classification for invasive papillary mucinous neoplasms. *Ann Surg Oncol*. 2011;18:644–650.

5. Murakami Y, Uemura K, Hayashidani Y, et al. Predictive factors of malignant or invasive intraductal papillary-mucinous neoplasms of the pancreas. *J Gastroitest Surg*. 2007;11:338–344.
6. Hwang DW, Jang JY, Lee SE, et al. Clinicopathologic analysis of surgically proven intraductal papillary mucinous neoplasms of the pancreas in SNUH: a 15-year experience at a single academic institution. *Langenbecks Arch Surg*. 2012;397:93–102.
7. Wasif N, Bentrem DJ, Farrell JJ, et al. Invasive intraductal papillary mucinous neoplasm versus sporadic pancreatic adenocarcinoma. *Cancer*. 2010;116:3369–3377.
8. Poultsides GA, Reddy S, Cameron JL, et al. Histopathologic basis for the favorable survival after resection of intraductal papillary mucinous neoplasm-associated invasive adenocarcinoma of the pancreas. *Ann Surg*. 2010;251:470–476.
9. Yopp AC, Katabi N, Janakos M, et al. Invasive carcinoma arising in intraductal papillary mucinous neoplasms of the pancreas. A matched control study with conventional pancreatic ductal adenocarcinoma. *Ann Surg*. 2011;253:968–974.
10. Schmidt CM, White PB, Waters JA, et al. Intraductal papillary mucinous neoplasms. Predictors of malignant and invasive pathology. *Ann Surg*. 2007;246:644–654.
11. Jang JY, Kim SW, Lee SE, et al. Treatment guidelines for branch duct type intraductal papillary mucinous neoplasms of the pancreas: when can we operate or observe? *Ann Surg Oncol*. 2007;15:199–205.
12. Akita H, Takeda Y, Hoshino H, et al. Mural nodule in branch duct-type intraductal papillary mucinous neoplasms of the pancreas is a marker of malignant transformation and indication for surgery. *Am J Surg*. 2011;202:214–219.
13. Shimizu Y, Kanemitsu Y, Sano T, et al. A nomogram for predicting the probability of carcinoma in patients with intraductal papillary mucinous neoplasm. *World J Surg*. 2010;34:2932–2938.
14. Salvia R, Crippa S, Falconi M, et al. Branch-duct intraductal papillary mucinous neoplasms of the pancreas: to operate or not to operate? *Gut*. 2007;56:1086–1090.
15. Cotton PB, Lehman G, Vennes J, et al. Endoscopic sphincterotomy complications and their management: an attempt at consensus. *Gastrointest Endosc*. 1991;37:383–393.
16. Weinberg BM, Spiegel BMR, Tomlinson JS, et al. Asymptomatic pancreatic cyst neoplasms: maximizing survival and quality of life using Markov-based clinical nomograms. *Gastroenterology*. 2010;138:531–540.
17. Tanaka M, Chari S, Adsay V, et al. International consensus guidelines for management of intraductal papillary mucinous neoplasms and mucinous cystic neoplasms of the pancreas. *Pancreatology*. 2006;6:17–32.
18. Maker AV, Lee LS, Raut CP, et al. Cytology from pancreatic cysts has marginal utility in surgical decision-making. *Ann Surg Oncol*. 2008;15:3187–3192.
19. Paris SA, Attasaranya S, Leblanc JK, et al. Role of endoscopic ultrasound in the diagnosis of intraductal papillary mucinous neoplasms: correlation with surgical histopathology. *Clin Gastroenterol Hepatol*. 2007;5:489–495.
20. Maire F, Voitot H, Aubert A, et al. Intraductal papillary mucinous neoplasms of the pancreas: performance of pancreatic fluid analysis for positive diagnosis and the prediction of malignancy. *Am J Gasetroenterol*. 2008;103:2871–2877.
21. Jong K, Poley JW, Hooft JE, et al. Endoscopic ultrasound-guided fine-needle aspiration of pancreatic cyst lesions provides inadequate material for cytology and laboratory analysis: initial results from a prospective study. *Endoscopy*. 2011;43:585–590.

Cancer Science
The official journal of the Japanese Cancer Association

Coexpression of MUC16 and mesothelin is related to the invasion process in pancreatic ductal adenocarcinoma

Atsushi Shimizu,[1] Seiko Hirono,[1,4] Masaji Tani,[1] Manabu Kawai,[1] Ken-Ichi Okada,[1] Motoki Miyazawa,[1] Yuji Kitahata,[1] Yasushi Nakamura,[2] Tetsuo Noda,[3] Shozo Yokoyama[1] and Hiroki Yamaue[1]

[1]Second Department of Surgery; [2]Department of Clinical Laboratory Medicine, Wakayama Medical University, Wakayama; [3]Cancer Institute, Japanese Foundation for Cancer Research, Tokyo, Japan

(Received November 18, 2011/Revised December 27, 2011/Accepted December 28, 2011/Accepted manuscript online February 9, 2012/Article first published online February 23, 2012)

The invasion process is a crucial step for pancreatic ductal adenocarcinoma (PDAC); however, the genes related to invasion remain unclear. To identify specific genes for the invasion process, we compared microarray data for infiltrating cancer and PanIN-3, which were harvested from an individual PDAC patient by microdissection. Furthermore, immunohistochemical, coimmunoprecipitation and invasion analyses were performed to confirm the biologic significance of molecules identified by expression profile. In the present study, we focused on MUC16 and mesothelin among 87 genes that were significantly upregulated in infiltrating components compared to PanIN-3 in all PDAC patients, because MUC16 was the most differently expressed between two regions, and mesothelin was reported as the receptor for MUC16. Immunohistochemical analysis revealed that MUC16 and mesothelin were expressed simultaneously only in infiltrating components and increased at the invasion front, and binding of MUC16 and mesothelin was found in PDAC by immunoprecipitation assay. The downregulation of MUC16 by shRNA and the blockage of MUC16 binding to mesothelin by antibody inhibited both invasion and migration of pancreatic cancer cell line. MUC16 high/mesothelin high expression was an independent prognostic factor for poor survival in PDAC patients. In conclusion, we identified two specific genes, MUC16 and mesothelin, associated with the invasion process in patients with PDAC. (*Cancer Sci* 2012; 103: 739–746)

For most patients with pancreatic ductal adenocarcinoma (PDAC), the diagnosis is made at an advanced stage;[1] the survival rate for these patients is dismal because PDAC has a propensity for early local invasion and vascular dissemination.[2] The genetic and biochemical determinants of the process of invasion and metastasis in PDAC are still largely unknown.

Pancreatic ductal adenocarcinoma appears to arise from histologically well-defined precursor lesions in the ducts of the pancreas, called pancreatic intraepithelial neoplasms (PanIN).[3,4] PanIN are graded based on their degree of architectural and nuclear atypia and are categorized into a four-tier classification, including PanIN-1A, 1B, 2 and 3.[5] PanIN-3 lesions demonstrate widespread loss of nuclear polarity, nuclear atypia and frequent mitoses, and whereas cancerous cells break through the basement membrane, they evolve into infiltrating adenocarcinoma. The invasion process is the crucial step in PDAC because cancer cells that invade the vasculature, or lymphatic or neural vessels, can progress further to metastasis only after obtaining infiltrating status. In the present study, we identified specific molecular markers associated with invasion in PDAC, which might be useful not only as early diagnostic markers but also as new therapeutic targets for patients with PDAC.

Several molecular markers, including tissue plasminogen activator,[6] artemin[7] and RhoGDI2,[8] have been reported to be associated with invasion in PDAC. However, some of these molecular markers are of little clinical value as therapeutic targets for patients with PDAC because these genes are also expressed in normal pancreatic tissues or other normal organs.[6–8] In this study, we first used a gene expression profiling technique to identify the specific genes that are differentially expressed between infiltrating cancer cells and PanIN-3 cells, which were harvested from an individual patient by laser microdissection. Based on our gene expression array data, clinical and biologic implications of MUC16 and mesothelin expression were further explored.

Material and Methods

Patients. Our study population included 103 patients with PDAC who underwent curative resection between January 2004 and December 2007 at Wakayama Medical University Hospital (WMUH). Informed consent was obtained from all patients in accordance with the guidelines of the Ethical Committee on Human Research of WMUH. Patient characteristics are presented in Table 1. The TNM staging criteria of the International Union Against Cancer was used for histologic classification.[9] None of the patients had received neoadjuvant chemotherapy or radiation therapy before surgery. The median follow-up duration after resection was 16.8 months (range: 1.6–67.3 months).

Laser microdissection and RNA extraction. Tissue samples including cancer cells and adjacent normal cells were embedded in Tissue-Tek OCT compound (Sakura Finetek, Torrance, CA, USA) by freezing tissue blocks in liquid nitrogen immediately after surgical resection for expression profiling. We used the tissues obtained from five patients with PDAC who had coexisting infiltrating cancer cells and PanIN-3 cells, and used the tissues from three patients as controls, including two patients with pancreatitis and one patient with bile duct cancer.

The specimens were cut into 9-μm sections at −20°C with the use of a LEICA cryostat (model 3050S; Leica, Tokyo, Japan) and then fixed on slides in 70% ethanol and stained with hematoxylin. The infiltrating cancer cells and PanIN-3 cells were harvested separately from an individual PDAC tissue using laser microdissection. As a control, the normal pancreatic duct cells were also obtained by laser microdissection, because PDAC originates from pancreatic ductal epithelial cells. Before laser microdissection, two pathologists (YS and

[4]To whom correspondence should be addressed.
E-mail: seiko-h@wakayama-med.ac.jp

doi: 10.1111/j.1349-7006.2012.02214.x

Table 1. Patient characteristics (n = 103)

Age, median (range)	69 (31–87)
Gender, male/female	54/49
Tumor site, Ph/Pbt/Phbt	71/30/2
Surgical technique, PD/DP/TP	71/30/2
Differentiation, well/moderate/poor	42/51/10
Tumor size	
≤20mm	18
>20 but ≤40mm	69
>40 but ≤60mm	14
>60mm	2
UICC stage	3
IA	3
IB	5
IIA	24
IIB	63
III	1
IV	7
Postoperative recurrence, yes/no	79/24

DP, distal pancreatectomy; Pbt, pancreatic body and tail; PD, pancreatoduodenectomy; Ph, pancreatic head; TP, total pancreatectomy; UICC, Union for International Cancer Control.

YN) diagnosed infiltrating cancer regions and PanIN-3 regions in the PDAC tissues, and normal pancreatic epithelium in normal pancreatic tissues. We estimated that the proportion of infiltrating cancer cells, PanIN-3 cells, or normal pancreatic ductal cells in the laser microdissected purified samples was at least 95%. Hence, we required more than 30 specimens (range, 35–78 specimens) in each sample for infiltrating cancer cells, more than 110 specimens (range, 111–414 specimens) for PanIN-3 cells and more than 450 specimens (range, 450–520 specimens) for normal pancreatic ductal epithelium cells to obtain enough RNA volume to use for our expression analysis. Total RNA was extracted from the harvested cells using the RNeasy Micro Kit (Qiagen, Hilden, Germany). The concentration of each total RNA sample was measured with a Nanodrop ND-1000 spectrophotometer (Nanodrop Technologies, Wilmington, DE, USA). The integrity of the RNA was determined by capillary electrophoresis using an Agilent 2100 Bioanalyzer (Agilent, Santa Clara, CA, USA) and the extracted RNA was accepted for experiments if the RNA integrity reading was >7.0.

Genome-wide transcriptional profiling. The gene expression was analyzed with Human Genome U133 Plus 2.0 GeneChips (Affymetrix, Santa Clara, CA, USA). The manufacturer's instructions regarding the protocols and the use of reagents for hybridization, washing and staining were followed (as previously described).[10] Data were collected using an Affymetrix GeneChip Scanner 3000 instrument. The cell intensity data files were obtained using the Affymetrix Suite 5.0 software program; then, the array data were imported into a DNA-Chip Analyzer (dChip, http://www.dchip.org) for high-level analysis.

Immunohistochemistry. Pretreatment was performed in a microwave using citrate buffer (pH 6.0) for 5 × 3 min at 700 W. Endogenous peroxidase activity was blocked with 3% hydrogen peroxide in methanol, and nonspecific binding sites were blocked with 10% normal goat serum. Primary antibodies were diluted in PBS: MUC16 (1:1000, mouse monoclonal, X325, Abcam, Cambridge, UK) and mesothelin (1:20, mouse monoclonal, 5B2, Novacastra, Newcastle upon Tyne, UK). Diluted primary antibodies were added, and samples were incubated overnight at 4°C. Antibody binding was then immunodetected using the avidin–biotin–peroxidase complex, as described by the supplier (Nichirei, Tokyo, Japan). Finally, the reaction products were demonstrated using a DAB substrate, and then counterstained with hematoxylin, dehydrated with ethanol and fixed with xylene.

To investigate the localization of the MUC16 and mesothelin, fluorescence immunohistochemistry was performed for paraffin-embedded tissue slides. Double labeling of the two mouse monoclonal antibodies (MUC16 [X325] and mesothelin [5B2]) was done using a Zenon kit (Molecular Probes, Eugene, OR, USA) to directly label the antibodies with either Alexa Fluor 488 or 594 according to the manufacturer's instructions.

Evaluation of immunohistochemistry. For scoring assessment, 200 cells were counted in each of the five different fields with high magnification, ×400, on the maximum cut surface of the tumor. We used ovarian cancer tissue and mesothelioma tissue as positive controls for MUC16 and mesothelin expression, respectively. The staining intensity was defined as follows: 0, no staining; 1+, weak; 2+, moderate; 3+, strong, based on the intensity levels of positive control being taken as 3+ (Fig. 1A).[11–13] If there were areas with a variety of staining intensities, the predominant intensity was chosen. The quantification of positivity (0–100%) was based on an estimate of the percentage of stained cancer cells in the lesion. The final immunostaining scores were calculated by multiplying the staining intensity and percentage positivity, thereby giving immunostaining scores ranging from 0 to 300.[14–17] The cut-off values of immunostaining scores were set as the median value, in accordance with previous reports.[18,19] The immunostains were scored by three investigators (SH, YN and HY) blinded to the clinical and pathologic data. If differences of opinion arose, a consensus was achieved by discussion.

Cell lines and RNA interference. Human pancreatic cancer cell line PK9 was obtained from the Cell Resource Center for Biomedical Research Institute of Development, Tohoku University (Miyagi, Japan).

Short hairpin RNA (shRNA) plasmids designed to target MUC16 were synthesized by SA Biosciences (Frederick, MD, USA) as follows: insert sequence ACAGCAGCATCAAGAGTTATT and ggaatctcattcgatgcatac (negative control). Each plasmid (0.8 μg) was mixed with 1 μL Lipofectamine2000 (Invitrogen, Carlsbad, CA, USA) in a final volume of 100 μL of Opti-MEM medium and was added to PK9 cells grown to 40% confluence in 24-well plates. Forty-eight hours after transfection, G418 solution (Roche, Basel, Switzerland) was added in the appropriate concentration. The stably transfected cells were maintained in RPMI-1640.

Coimmunoprecipitation assay. To address binding between MUC16 and mesothelin, we performed coimmunoprecipitation assays using pancreatic cancer cell line PK9 and two surgical specimens obtained from 2 PDAC patients. The coimmunoprecipitation assays were performed using the Universal Magnetic Co-IP Kit (Active Motif, Rixensart, Belgium) according to the manufacturer's protocol. Monoclonal antibody against CA125 (OC125, Abcam, Cambridge, UK), monoclonal antibody against mesothelin (MN-1, Rockland, Gilbertsville, PA, USA) or rabbit IgG control (Abcam) were used for immunoprecipitation and immunoblotting.

***In vitro* invasion and migration assay in PK9 cell line transfected with MUC16 shRNA.** To investigate the effect of MUC16 expression on invasion and migration of pancreatic cancer cells, *in vitro* invasion and migration assays were performed in the membrane culture system using an 8-μm pore size PET membrane coated with or without Matrigel (24-well, BD Biosciences, San Diego, CA, USA). Parental PK9 cells, vector control-PK9 cells and PK9 cells transfected with MUC16 shRNA were seeded into 5 × 10^4 cells/500 μL growth medium on the Matrigel layer. The following procedures were performed (as previously described).[20]

doi: 10.1111/j.1349-7006.2012.02214.x

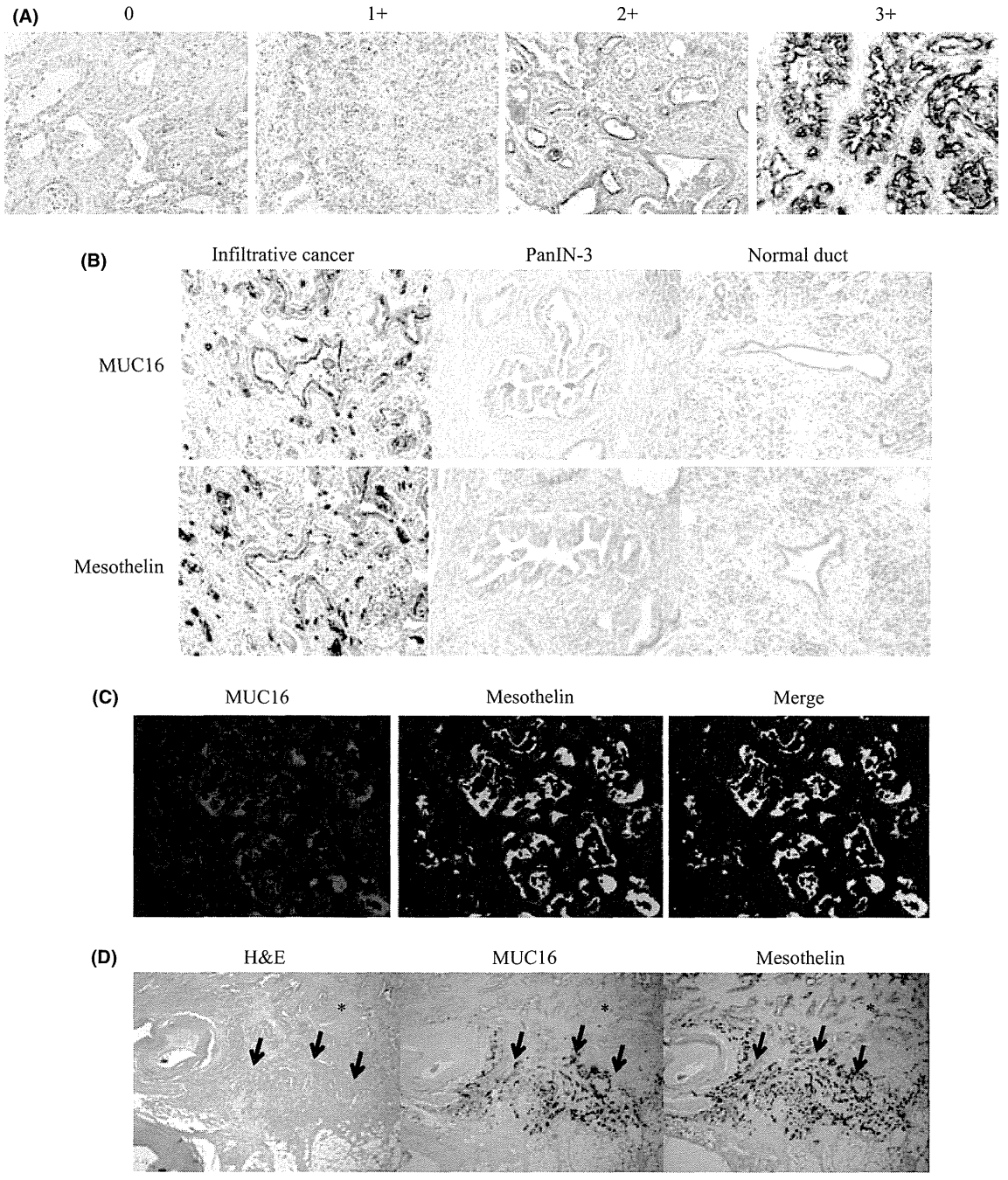

Fig. 1. (A) Image of staining intensity grade. (0) no staining, (1+) weak, (2+) moderate, (3+) strong intensity. (B) MUC16 and mesothelin were stained at the apical membrane or cytoplasm only in infiltrative cancer, whereas no staining appeared in PanIN-3 cells and normal ductal cells. (C) MUC16 and mesothelin expressed at the apical cancer cell surface in invasive ductal cancer cells labeled with Zenon Alexa Fluor 594 and 488. The merged image shows MUC16 and mesothelin expressed in the same cancer cells simultaneously. (D) The expression of MUC16 and mesothelin was higher at the invasion front (arrow) than in the main tumor (*). H&E, hematoxylin and eosin stain.

***In vitro* invasion and migration assays with blocking antibodies for MUC16 and mesothelin.** To investigate the binding between MUC16 and mesothelin, we evaluated the effect of blocking antibodies against interaction between MUC16 and mesothelin on invasion and migration of pancreatic cancer cell PK9 by using *in vitro* invasion and migration assay. Because OC125 (DAKO, Carpinteria, CA, USA) and M11 (DAKO) are known to block the interaction between MUC16 and mesothelin,[21] each antibody was used for blocking the interaction. Sodium azide was removed using the AbSelect Antibody Purification System (Innova Biosciences, Cambridge, UK).

Statistical analysis. The association between MUC16/mesothelin expression and clinicopathologic factors in the patients with PDAC was assessed using the χ^2-test or the Fisher exact test. The survival curves were calculated using the Kaplan–Meier method and then compared by means of the log-rank test. The prognostic significance of clinicopathologic features and MUC16/mesothelin expression was determined using univariate Cox regression analysis. Cox proportional hazards models were fitted for multivariate analysis. Statistical procedures were performed using SPSS version 13.0 (SPSS, Chicago, IL, USA). $P < 0.05$ was considered statistically significant.

Results

Identification of the transcriptional biomarkers associated with the invasion of pancreatic ductal adenocarcinoma by gene expression profiling. Microarray data for the infiltrating cancer and PanIN-3, which were harvested from an individual PDAC patient, were compared on the basis of the following criteria: (i) a ≥ 1.5-fold change in the expression levels between the infiltrating cells and PanIN-3 cells; (ii) a >100 absolute difference between the expression levels of the infiltrating cells and PanIN-3 cells; and (iii) $P < 0.05$.[22,23] A total of 109 genes were differentially expressed between infiltrating cancer and PanIN-3 cells in PDAC, including 87 genes that were upregulated and 22 that were downregulated in the infiltrating PDAC, and then 18 genes, which were expressed more in both infiltrating cancer and PanIN3 than in normal pancreatic epithelium, were listed (see Table 2), to focus on more significant genes related to carcinogenesis in PDAC. Among the upregulated genes identified by expression profiling, we focused on MUC16 because MUC16 expression in the infiltrating cancer was substantially higher than that of the PanIN-3 cells in all five PDAC patients and normal pancreatic duct epithelium (Table 2), indicating that MUC16 is specifically expressed in invasive PDAC. We also focused on mesothelin in the upregulates genes list, because it had been previously reported to be a ligand receptor of MUC16.[24,25]

Immunohistochemical staining of MUC16 and mesothelin in pancreatic ductal adenocarcinoma. The immunohistochemical analyses were performed in the paraffin-embedded tissues from 103 patients with PDAC. MUC16 and mesothelin were stained by immunohistochemistry at the tumor apical membrane or cytoplasm (or both) in PDAC samples (Fig. 1B). Both MUC16 and mesothelin were expressed only in the infiltrating cancer cells and not in the PanIN-3 cells ($n = 30$) or normal pancreatic epithelial cells ($n = 103$) (Fig. 1B). Furthermore, we found that these genes were not expressed in any non-epithelial cells, including stromal cells, acinar cells and islet cells. Fluorescence immunohistochemistry using the merge technique showed that MUC16 and mesothelin were stained in the same cancer cells simultaneously (Fig. 1C). We observed that MUC16 and mesothelin were more highly expressed at the invasion front than in the main tumor in 48 of the 103 patients (47%) with PDAC (Fig. 1D).

The scores of MUC16 and mesothelin expression were calculated for each sample. The median scores of MUC16 and mesothelin were 150 (range, 0–300) and 180 (range, 0–300), respectively. The binarization of the score data for these markers was performed as "high expression" versus "low expression" at the median level. We categorized all samples into two groups to analyze the association of MUC16 and mesothelin expression with the clinicopathologic features in the patients with PDAC: the MUC16 high/mesothelin high expression group ($n = 41$) versus the other group ($n = 62$), which included the patients with MUC16 high/mesothelin low expression ($n = 11$), those with MUC16 low/mesothelin high expression ($n = 11$) and MUC16 low/mesothelin low expression ($n = 40$).

Association of MUC16 and mesothelin expression with pathologic factors. The correlation of pathologic factors and MUC16/mesothelin expression was analyzed (Table 3). These pathologic factors were evaluated in accordance with the second English edition of the Classification of Pancreatic Carcinoma, proposed by the Japan Pancreas Society.[26] The analysis indicated that a tumor size >4.0 cm, serosal invasion, invasion of other organs, and lymphatic permeation occurred significantly more often in the MUC16 high/mesothelin high expression group than in the other groups ($P = 0.0041$, $P = 0.0131$, $P = 0.0356$ and $P = 0.0250$, respectively).

Binding of MUC16 and mesothelin in pancreatic cancer cell PK9 and surgical specimens from patients with pancreatic ductal adenocarcinoma. The coimmunoprecipitation assays between MUC16 and mesothelin using pancreatic cancer cell line PK9 and surgical specimens obtained from two PDAC patients (number 1: stage IIB, number 2: stage IV) showed that the whole cell lysates or tissue homogenates were immunoprecipitated and immunoblotted with anti-MUC16 and anti-mesothelin antibody (Fig. 2A), indicating that MUC16 and mesothelin can bind in PDAC.

Role of MUC16 and mesothelin in invasion, migration and cell growth of pancreatic cancer cell line. PK9 cells express MUC16 and were transfected with shRNA targeted to MUC16. Stable

Table 2. Upregulated genes in the infiltrating cancer compared to PanIN-3 component of pancreatic ductal adenocarcinoma as determined by expression profiling

Probe ID	Gene name	Gene symbol	Fold change, mean	Mean expression level	
				IC/PanIN-3	IC/normal
220196_at	Mucin 16	MUC16	26.7	14.6	31.6
206884_s_at	Sciellin	SCEL	17.4	3.8	4.7
205388_at	Troponin C type 2	TNNC2	10.1	4.1	10.0
204416_x_at	Apolipoprotein C-I	APOC1	6.7	5.9	7.2
213524_s_at	G0/G1switch 2	G0S2	5.4	4.3	13.9
202504_at	Tripartite motif-containing 29	TRIM29	4.5	2.6	8.8
204070_at	Retinoic acid receptor responder 3	RARRES3	3.7	3.4	5.4
242625_at	Radical S-adenosyl methionine domain containing 2	RSAD2	3.6	2.4	12.1
204885_s_at	Mesothelin	MSLN	3.0	2.2	2.2
201564_s_at	Fascin homolog 1, actin-bundling protein	FSCN1	3.0	2.7	3.1
205483_s_at	Interferon, alpha-inducible protein	IFI	3.0	2.5	7.6
228640_at	BH-protocadherin	PCDH7	2.7	2.5	7.5
239979_at	Epithelial stromal interaction 1	EPSTI1	2.5	2.1	6.5
231956_at	KIAA1618	KIAA1618	2.4	2.4	3.8
204285_s_at	Phorbol-12-myristate-13-acetate-induced protein 1	PMAIP1	2.2	2.1	3.4
222810_s_at	RAS protein activator like 2	RASAL2	2.2	2.2	2.3
243271_at	Sterile alpha motif domain containing 9-like	SAMD9L	2.1	1.9	5.7
200736_s_at	Glutathione peroxidase 1	GPX1	2.0	1.9	2.0

IC, infiltrating cancer; PanIN, pancreatic intraepithelial neoplasms.

doi: 10.1111/j.1349-7006.2012.02214.x

Table 3. The association of MUC16 and mesothelin expression with pathologic factors in patients with pancreatic ductal adenocarcinoma

	Number	MUC16 high/ mesothelin high group	Other group	*P*
		41	62	
Differentiation				
Well/ moderate	93	35	57	0.1908
Poor	10	6	4	
Tumor size				
>40mm	16	12	4	0.0041
≤40mm	87	29	58	
Local progression				
Intrapancreatic common bile duct invasion				
Positive	22	6	16	0.1757
Negative	81	35	46	
Duodenal invasion				
Positive	40	12	28	0.1052
Negative	63	29	34	
Serosal invasion				
Positive	74	35	39	0.0131
Negative	29	6	23	
Retropancreatic tissue invasion				
Positive	85	35	50	0.5369
Negative	18	6	12	
Portal venous system invasion				
Positive	25	13	12	0.1523
Negative	78	28	50	
Arterial system invasion				
Positive	5	4	1	0.0803
Negative	98	37	61	
Extrapancreatic nerve plexus invasion				
Positive	33	16	17	0.2166
Negative	70	25	45	
Invasion of other organs				
Positive	6	5	1	0.0356
Negative	97	36	61	
Lymphatic permeation				
Positive	88	39	49	0.0250
Negative	15	2	13	
Vascular permeation				
Positive	64	28	36	0.2948
Negative	39	13	26	
Perineural invasion				
Positive	76	29	47	0.5665
Negative	27	12	15	
Lymph node metastasis				
Positive	69	32	37	0.0523
Negative	34	9	25	

MUC16–shRNA-transfected PK9 cells showed downregulation of MUC16 protein expression compared to the vector control (data not shown). Invasion chamber experiments revealed that MUC16–shRNA-transfected PK9 cells had significant suppression of cell invasion (Fig. 2B). Migration assays also demonstrated that downregulation of MUC16 significantly reduced migration (Fig. 2C). The blockage of MUC16 binding to mesothelin with the neutralizing antibodies against MUC16 (OC125 or M11) significantly suppressed invasion and migration of pancreatic cancer cells (Fig. 2D,E). In terms of the effect of MUC16 on cell growth, parental PK9 cells, vector control-PK9 cells and MUC16–shRNA-transfected PK9 were seeded in concentration of 10×10^4/mL, and the cell numbers were counted on day 1, 3 and 5 using a hemocytometer. As a result, the cell growth was significantly suppressed after inhibition of MUC16 expression (Fig. 2F).

Association of MUC16 and mesothelin expression with survival in patients with pancreatic ductal adenocarcinoma. The overall survival of the MUC16 high/mesothelin high expression group was significantly worse than in the other group (median 11.9 *vs* 22.8 months, $P = 0.0006$; Fig. 3A). The 1-, 3- and 5-year survival rates of the MUC16 high/mesothelin high group versus the other group were as follows: 51.2 *vs* 72.6%, 8.0 *vs* 25.6% and 0 *vs* 11.5%, respectively. The disease-free survival of the MUC16 high/mesothelin high expression group was also worse than the other group (median 6.7 *vs* 10.9 months, $P = 0.0002$; Fig. 3B). The 1-, 3- and 5-year disease-free survival rates of the MUC16 high/mesothelin high group versus the other group were as follows: 12.2 *vs* 48.4%, 2.5 *vs* 20.3% and 0 *vs* 11.5%, respectively. In the univariate analysis of the overall survival of the patients with PDAC, a tumor size > 4.0 cm, duodenal invasion, portal venous system invasion, lymphatic permeation, vascular permeation, lymph node metastasis and MUC16 high/mesothelin high expression were potential factors for predicting poor survival (Table 4). According to a multivariate analysis of overall survival, vascular permeation and MUC16 high/mesothelin high expression were independent factors for predicting short survival for the patients with PDAC ($P = 0.0025$, HR, 2.241; 95% CI, 1.364–4.310; $P = 0.0158$, HR, 1.936; 95%CI, 1.132–3.310, respectively; Table 4). Similarly, in the multivariate analysis of disease-free survival, a tumor size > 4.0 cm, lymphatic permeation and MUC16 high/mesothelin high expression were independent prognostic factors for a poorer disease-free survival ($P = 0.0167$, HR, 2.141, 95% CI, 1.148–4.000; $P = 0.0202$, HR, 3.984, 95% CI, 1.241–12.821; $P = 0.0131$, HR, 1.985, 95% CI, 1.155–3.412, respectively; Table 5).

Discussion

We first identified genes specific to the invasion process in PDAC using microdissection and gene expression profiling techniques. In this study, we compared microarray data of infiltrating cancer and PanIN3, which were harvested from an individual PDAC patient, to exclude the difference in original gene expression among individuals. Then, we were able to identify similar genes that were differently expressed between infiltrating cancer and PanIN-3 in all five patients.

Among the identified upregulated genes, we focused on MUC16 because its expression in the infiltrating cancer was substantially higher than that in the PanIN-3 cells. We also focused on mesothelin in the list, because it was reported to be a ligand receptor of MUC16. Their interaction has been postulated to play an important role during tumorigenesis and metastasis in ovarian cancer.[24,25] Rump and colleagues reported that the binding of MUC16 and mesothelin expressed by cancer cells mediates heterotypic cell adhesion and might contribute to the metastasis and invasion of ovarian cancer.[24]

In the present study, immunohistochemical analysis revealed that MUC16 and mesothelin were expressed in the infiltrating cancer cells but not in the PanIN-3 cells or normal pancreatic tissues, consistent with the results of gene expression profiling. Furthermore, fluorescence immunohistochemistry showed that MUC16 and mesothelin were expressed simultaneously in the PDAC cells.

MUC16 encodes the CA125 antigen and is a membrane-bound mucin protein with a high molecular weight between 2.5 and 5.0 million daltons.[27] Its proposed structure comprises an N-terminal domain of >22 000 amino acid residues that are presumably heavily glycosylated, a central domain containing up to 60 glycosylated repeat sequences constituting

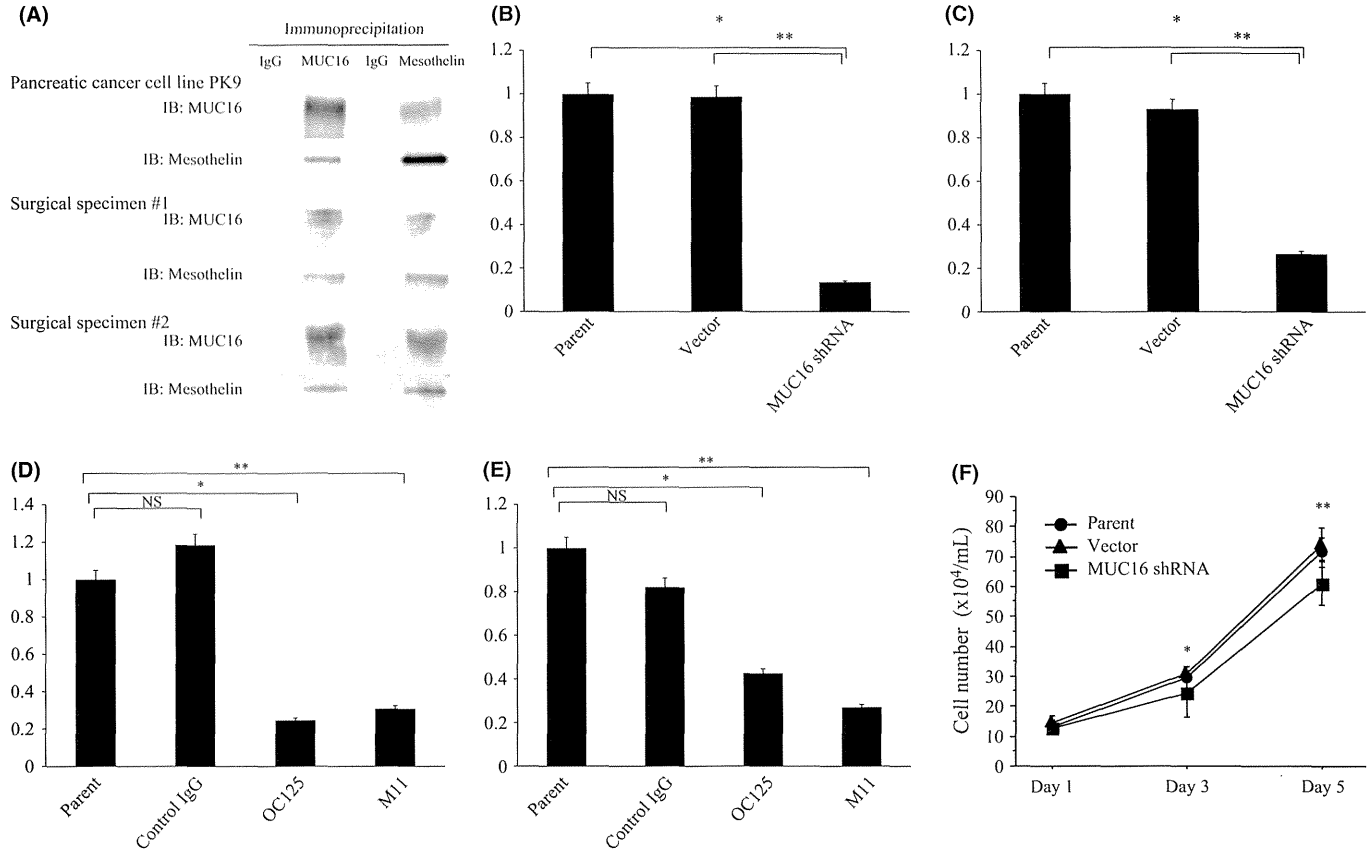

Fig. 2. (A) The results of coimmunoprecipitation assay in pancreatic cancer cell line PK9 and clinical samples from the patients with pancreatic ductal adenocarcinoma. The whole cell lysates extracted from cell line or tissue homogenates extracted from two surgical specimens were immunoprecipitated and immunoblotted with anti-MUC16 and anti-mesothelin antibody. IB, immunoblotting. (B) Invasion chamber experiments in PK9 transfected with MUC16 shRNA. The invasion was significantly suppressed after inhibition of MUC16 expression (*P = 0.0009, **P = 0.0067). (C) Migration assays in PK9 transfected with MUC16 shRNA. The migration was significantly suppressed after downregulation of MUC16 expression (*P = 0.0005, **P = 0.0055). (D) Invasion assay with the blockage of MUC16 binding to mesothelin with the neutralizing antibodies against MUC16 (OC125 or M11, *P = 0.0014, **P = 0.0043). (E) Migration assay with the blockage of MUC16 binding to mesothelin with OC12 5 or M11 (*P = 0.0020, **P = 0.0003). (F) Cell growth assay in PK9 transfected with MUC16 shRNA. The cell growth was significantly suppressed after inhibition of MUC16 expression (*P = 0.0469, **P = 0.0036). NS, not significant.

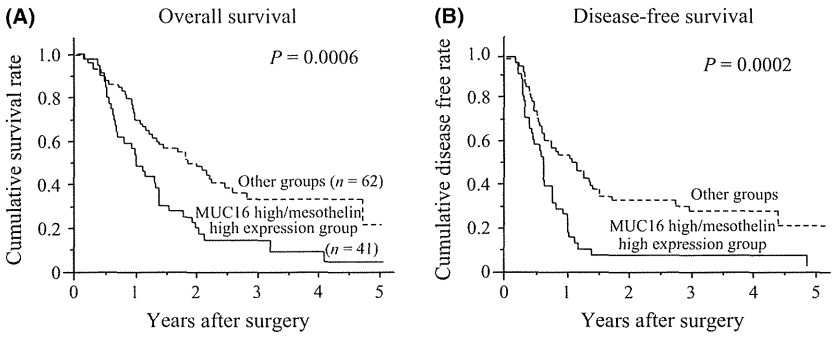

Fig. 3. The overall survival (A) and disease-free survival (B) of the MUC16 high/mesothelin high expression group was worse than that of the other groups (median, 11.9 *vs* 22.8 months, P = 0.0006; 6.7 *vs* 10.9 months, P = 0.0002, respectively).

the tandem repeats characteristic of mucins, and a C-terminal domain composed of a transmembrane domain and a short cytoplasmic tail with possible phosphorylation sites.[28] Few reports have described the expression of MUC16 in cancers. In this study, using immunohistochemistry, we detected the expression of MUC16 in 94 of 103 PDAC cases (91%).

The mesothelin gene encodes a 71-kDa precursor protein that is processed into the 40-kDa glycosylphosphatidylinositol-anchored membrane glycoprotein, mesothelin and a 31-kDa fragment called megakaryocyte potentiating factor.[29,30] Mesothelin expression in normal human tissues is limited to mesothelial cells lining the pleura, pericardium and peritoneum,[29] and the protein is also expressed by a variety of solid tumors, including ovarian cancer, malignant mesothelioma, lung cancer and PDAC.[31,32] Mesothelin expression reportedly conferred chemoresistance and a poorer clinical outcome in ovarian cancer patients.[33]

We found that the coexpression of MUC16 and mesothelin was also increased at the invasion front (n = 48), compared to that in the main tumor in several PDAC tissues, and, then, MUC16 high/mesothelin high expression in PDAC was significantly associated with large tumors, serosal invasion, invasion of other organs and lymphatic permeation. These results indicate that these molecules seem to be involved in invasion and

doi: 10.1111/j.1349-7006.2012.02214.x

Table 4. Univariate and multivariate analysis using the Cox proportional hazards regression model of overall survival in 103 patients with pancreatic ductal adenocarcinoma

	Univariate analysis			Multivariate analysis		
	P	HR	95% CI	*P*	HR	95% CI
Age, ≥70	0.2692	0.906	0.962–1.011	–	–	–
Gender, male	0.7711	1.026	0.678–1.689	–	–	–
Differentiation, poor	0.9228	1.043	0.451–2.410	–	–	–
Tumor size, > 40 mm	0.0070	2.203	1.241–3.906	0.3294	1.340	0.743–2.421
Local progression						
CH, positive	0.1651	1.458	0.856–2.481	–	–	–
DU, positive	0.0465	1.595	1.007–2.525	0.0782	1.575	0.950–2.604
S, positive	0.3320	1.297	0.767–2.188	–	–	–
RP, positive	0.0715	1.848	0.948–3.610	–	–	–
PV, positive	0.0203	1.818	1.098–3.012	0.6830	1.119	0.653–1.916
A, positive	0.6183	1.259	0.507–3.135	–	–	–
PL, positive	0.0666	1.543	0.971–2.451	–	–	–
OO, positive	0.4899	1.342	0.581–3.101	–	–	–
Lymphatic permeation, positive	0.0034	3.937	1.575–9.804	0.1190	2.375	0.801–7.042
Vascular permeation, positive	< 0.0001	3.155	1.859–5.348	0.0025	2.421	1.364–4.310
Perineural invasion, positive	0.1345	1.527	0.877–2.660	–	–	–
Lymph node metastasis, positive	0.0043	2.151	1.272–3.636	0.8436	1.067	0.561–2.033
MUC16/mesothelin expression, high	0.0008	2.206	1.392–3.495	0.0158	1.936	1.132–3.310

A, arterial system invasion; CH, intrapancreatic common bile duct invasion; CI, confidence interval; DU, duodenal invasion; HR, hazard ratio; OO, invasion of other organs; PL, extrapancreatic nerve plexus invasion; PV, portal venous system invasion; RP, retropancreatic tissue invasion; S, serosal invasion.

Table 5. Univariate and multivariate analysis using the Cox proportional hazards regression model of disease-free survival in 103 patients with pancreatic ductal adenocarcinoma

	Univariate analysis			Multivariate analysis		
	P	HR	95% CI	*P*	HR	95% CI
Age, ≥70	0.5105	1.161	0.743–1.815	–	–	–
Gender, male	0.9862	0.996	0.638–1.555	–	–	–
Differentiation, poor	0.5830	0.792	0.344–1.825	–	–	–
Tumor size, > 40 mm	0.0001	3.257	1.770–5.988	0.0167	2.141	1.148–4.000
Local progression						
CH, positive	0.6377	1.138	0.664–1.953	–	–	–
DU, positive	0.0105	1.805	1.148–2.833	0.0633	1.590	0.975–2.591
S, positive	0.0864	1.605	0.935–2.755	–	–	–
RP, positive	0.1104	1.689	0.887–3.205	–	–	–
PV, positive	0.0410	1.675	1.021–2.755	0.6492	1.136	0.656–1.965
A, positive	0.8599	1.095	0.397–3.021	–	–	–
PL, positive	0.2523	1.316	0.822–2.110	–	–	–
OO, positive	0.7087	1.189	0.479–2.959	–	–	–
Lymphatic permeation, positive	0.0034	3.937	2.370–18.181	0.0202	3.984	1.241–12.821
Vascular permeation, positive	0.0012	2.198	1.362–3.546	0.1429	1.506	0.871–2.604
Perineural invasion, positive	0.0452	1.736	1.012–2.985	0.1162	1.577	0.894–2.778
Lymph node metastasis, positive	< 0.0001	3.778	1.938–5.917	0.2388	1.484	0.770–2.857
MUC16/mesothelin expression, high	0.0002	2.378	1.497–3.777	0.0131	1.985	1.155–3.412

A, arterial system invasion; CH, intrapancreatic common bile duct invasion; CI, confidence interval; DU, duodenal invasion; HR, hazard ratio; OO, invasion of other organs; PL, extrapancreatic nerve plexus invasion; PV, portal venous system invasion; RP, retropancreatic tissue invasion; S, serosal invasion.

migration of pancreatic cancer cells. Recent reports show the role of MUC16 in ovarian cancer tumorigenesis,[34,35] and it has been noted that MUC16 regulates cell growth, invasion and metastasis in epithelial ovarian cancer.[34] However, another report indicates the opposite concept, that downregulation of MUC16 inhibits invasion and migration due to the suppression of epithelial to mesenchymal transition in ovarian cancer cells.[35] Thus, the role of MUC16 in ovarian cancer cell invasion and migration is still controversial and no report regarding the role of MUC16 on pancreatic cancer cell invasion and migration has yet appeared.

To examine the role of interaction of MUC16 and mesothelin on pancreatic cancer invasion and migration, we investigated whether shRNA and blocking antibodies for MUC16 suppress invasion and migration of pancreatic cancer cells. We investigated the expression of MUC16 and mesothelin by RT-PCR, western blotting and immunocytochemistry in eight pancreatic cancer cell lines (PK9, PANC1, MIAPaCa2, AsPC1, BxPC3, Capan-1, Capan-2 and PK1). By RT-PCR, both MUC16 and mesothelin mRNAs were detected in five cell lines, including PK9, AsPC1, BxPC3, Capan-2 and PK1. Using western blotting and immunocytochemistry, the strongest positive

expressions of both MUC16 and mesothelin were found in PK9. Therefore, in the present study, we used only PK9 cell line for biological experiments. The blockage of the interaction between MUC16 and mesothelin suppressed invasion and migration of pancreatic cancer cells, suggesting that MUC16 binding to mesothelin is important for cell invasion and migration in pancreatic cancer cells.

Furthermore, we focused on the survival of patients with MUC16 high and mesothelin high expression because coexpression of these two genes is obviously correlated to the invasion of PDAC, and MUC16 high/mesothelin high expression was an independent prognostic factor for poor survival. We examined whether there are any differences in survival between the MUC16 high/mesothelin high group and the MUC16 high/mesothelin low group or MUC16 low/mesothelin high group. However, these groups were very small ($n = 11$), and larger groups of patients are necessary for further study.

The mechanism of overexpression of MUC16 and mesothelin in PDAC has not yet been clarified yet. It is also unclear whether the coexpression of MUC16 and mesothelin was coincidental or the increased expression of MUC16 was associated with an upregulation of mesothelin expression. These issues should be clarified in further studies. Moreover, other molecules in Table 2 besides MUC16 and mesothelin might potentially contribute to the invasion process. In the future, we analyze the roles of other upregulated genes in infiltrating cancer than in PanIN-3 for PDAC patients.

In conclusion, MUC16 and mesothelin are involved in pancreatic cancer cell invasion and migration, and MUC16 and mesothelin clinically represent new prognostic biomarkers for PDAC and might be new therapeutic targets for patients with PDAC, including immunotherapy using a peptide vaccine or monoclonal antibody therapy.

Acknowledgments

This study was supported by Grant-in-Aid no.19390341 and 22791297 from the Ministry of Education, Culture, Sports, Science and Technology of Japan.

Disclosure Statement

The authors have no conflict of interest.

References

1 Hidalgo M. Pancreatic cancer. *N Engl J Med* 2010; **362**: 1605–17.
2 Dumartin L, Quemener C, Laklai H *et al.* Netrin-1 mediates early events in pancreatic adenocarcinoma progression, acting on tumor and endothelial cells. *Gastroenterology* 2010; **138**: 1595–606.
3 Hruban RH, Goggins M, Parsons J Kern SE. Progression model for pancreatic cancer. *Clin Cancer Res* 2000; **6**: 2969–72.
4 Hruban RH, Adsay NV, Albores-Saavedra J *et al.* Pancreatic intraepithelial neoplasia: a new nomenclature and classification system for pancreatic duct lesions. *Am J Surg Pathol* 2001; **25**: 579–86.
5 Kern S, Hruban R, Hollingsworth MA *et al.* A white paper: the product of a pancreas cancer think tank. *Cancer Res* 2001; **61**: 4923–32.
6 Diaz VM, Hurtado M, Thomson TM, Reventos J, Paciucci R. Specific interaction of tissue-type plasminogen activator (t-PA) with annexin II on the membrane of pancreatic cancer cells activates plasminogen and promotes invasion in vitro. *Gut* 2004; **53**: 993–1000.
7 Ceyhan GO, Giese NA, Erkan M *et al.* The neurotrophic factor artemin promotes pancreatic cancer invasion. *Ann Surg* 2006; **244**: 274–81.
8 Abiatari I, DeOliveira T, Kerkadze V *et al.* Consensus transcriptome signature of perineural invasion in pancreatic carcinoma. *Mol Cancer Ther* 2009; **8**: 1494–504.
9 Sobin LH, Wittekind CH. *International Union Against Cancer: TNM Classification of Malignant Tumors*, 6th edn. New York, NY: Wiley and Liss, 2002.
10 Hirono S, Yamaue H, Hoshikawa Y *et al.* Molecular markers associated with lymph node metastasis in pancreatic ductal adenocarcinoma by genome-wide expression profiling. *Cancer Sci* 2010; **101**: 259–66.
11 McClelland RA, Finlay P, Walker KJ *et al.* Automated quantitation of immunocytochemically localized estrogen receptors in human breast cancer. *Cancer Res* 1990; **50**: 3545–50.
12 Detre S, Saclani Jotti G, Dowsett M. A "quickscore" method for immunohistochemical semiquantitation: Validation for oestrogen receptor in breast carcinomas. *J Clin Pathol* 1995; **48**: 876–8.
13 Allred DC, Harvey JM, Berardo M, Clark GM. Prognostic and predictive factors in breast cancer by immunohistochemical analysis. *Mod Pathol* 1998; **11**: 155–68.
14 Campagna D, Cope L, Lakkur SS, Henderson C, Laheru D, Iacobuzio-Donahue CA. Gene expression profiles associated with advanced pancreatic cancer. *Int J Clin Exp Pathol* 2008; **1**: 32–43.
15 Fritsche P, Seidler B, Schuler S *et al.* HDAC2 mediates therapeutic resistance of pancreatic cancer cells via the BH3-only protein NOXA. *Gut* 2009; **58**: 1399–409.
16 Meinhold-Heerlein I, Stenner-Liewen F, Liewen H *et al.* Expression and potential role of Fas-associated phosphatase-1 in ovarian cancer. *Am J Pathol* 2001; **158**: 1335–44.
17 Seethala RR, Gooding WE, Handler PN *et al.* Immunohistochemical analysis of phosphotyrosine signal transducer and activator of transcription 3 and epidermal growth factor receptor autocrine signaling pathways in head and neck cancers and metastatic lymph nodes. *Clin Cancer Res* 2008; **14**: 1303–9.
18 Campbell EJ, McDuff E, Tatarov O *et al.* Phosphorylated c-Src in the nucleus is associated with improved patient outcome in ER-positive breast cancer. *Br J Cancer* 2008; **99**: 1769–74.
19 Cappia S, Righi L, Mirabelli D *et al.* Prognostic role of osteopontin expression in malignant pleural mesothelioma. *Am J Clin Pathol* 2008; **130**: 58–64.
20 Ieda J, Yokoyama S, Tamura K *et al.* Re-expression of CEACAM1 long cytoplasmic domain isoform is associated with invasion and migration of colorectal cancer. *Int J Cancer* 2011; **129**: 1351–61.
21 Scholler N, Garvik B, Hayden-Ledbetter M, Kline T, Urban N. Development of a CA125-mesothelin cell adhesion assay as a screening tool for biologics discovery. *Cancer Lett* 2007; **8**: 130–6.
22 Gronborg M, Kristiansen TZ, Iwahori A *et al.* Biomarker discovery from pancreatic cancer secretome using a differential proteomic approach. *Mol Cell Proteomics* 2006; **5**: 157–71.
23 Yamanaka S, Sunamura M, Furukawa T *et al.* Chromosome 12, frequently deleted in human pancreatic cancer, may encode a tumor-suppressor gene that suppresses angiogenesis. *Lab Invest* 2004; **84**: 1339–51.
24 Rump A, Morikawa Y, Tanaka M *et al.* Binding of ovarian cancer antigen CA125/MUC16 to mesothelin mediates cell adhesion. *J Biol Chem* 2004; **279**: 9190–8.
25 Gubbels JA, Belisle J, Onda M *et al.* Mesothelin-MUC16 binding is a high affinity, N-glycan dependent interaction that facilitates peritoneal metastasis of ovarian tumors. *Mol Cancer* 2006; **5**: 50.
26 Japan Pancreas Society. *Classification of Pancreatic Carcinoma*, 2nd English edn. Tokyo: Kanahara, 2003.
27 Yin BW, Lloyd KO. Molecular cloning of the CA125 ovarian cancer antigen: identification as a new mucin, MUC16. *J Biol Chem* 2001; **276**: 27371–5.
28 O'Brien TJ, Beard JB, Underwood LJ, Shigemasa K. The CA 125 gene: a newly discovered extension of the glycosylated N-terminal domain doubles the size of this extracellular superstructure. *Tumor Biol* 2002; **23**: 154–69.
29 Chang K, Pastan I, Willingham MC. Isolation and characterization of a monoclonal antibody, K1, reactive with ovarian cancers and normal mesothelium. *Int J Cancer* 1992; **50**: 373–81.
30 Hassan R, Bera T, Pastan I. Mesothelin: a new target for immunotherapy. *Clin Cancer Res* 2004; **10**(12 Pt 1): 3937–42.
31 Ordonez NG. Application of mesothelin immunostaining in tumor diagnosis. *Am J Surg Pathol* 2003; **27**: 1418–28.
32 Argani P, Iacobuzio-Donahue CA, Ryu B *et al.* Mesothelin is overexpressed in the vast majority of ductal adenocarcinomas of the pancreas: identification of a new pancreatic cancer marker by serial analysis of gene expression (SAGE). *Clin Cancer Res* 2001; **7**: 3862–8.
33 Cheng WF, Huang CY, Chang MC *et al.* High mesothelin correlates with chemoresistance and poor survival in epithelial ovarian carcinoma. *Br J Cancer* 2009; **100**: 1144–53.
34 Thériault C, Pinard M, Comamala M *et al.* MUC16 (CA125) regulates epithelial ovarian cancer cell growth, tumorigenesis and metastasis. *Gynecol Oncol* 2011; **121**: 434–43.
35 Comamala M, Pinard M, Thériault C *et al.* Downregulation of cell surface CA125/MUC16 induces epithelial-to-mesenchymal transition and restores EGFR signaling in NIH:OVCAR3 ovarian carcinoma cells. *Br J Cancer* 2011; **104**: 989–99.

doi: 10.1111/j.1349-7006.2012.02214.x

Original Paper

Digestive Surgery

Dig Surg 2012;29:132–139
DOI: 10.1159/000337306

Received: October 19, 2011
Accepted after revision: February 13, 2012
Published online: April 24, 2012

Identification of the Lymphatic Drainage Pathways from the Pancreatic Head Guided by Indocyanine Green Fluorescence Imaging during Pancreaticoduodenectomy

Seiko Hirono Masaji Tani Manabu Kawai Ken-ichi Okada Motoki Miyazawa
Atsushi Shimizu Kazuhisa Uchiyama Hiroki Yamaue

Second Department of Surgery, Wakayama Medical University School of Medicine, Wakayama, Japan

Key Words
Lymphatic drainage pathway · Pancreatic head · Indocyanine green fluorescence imaging · Optimal lymphadectomy for pancreatic cancer

Abstract
Aims: We identified the lymphatic drainage pathways from the pancreatic head guided by indocyanine green (ICG) fluorescence imaging to analyze optimal lymphadectomy for pancreatic cancer. ***Methods:*** The lymphatic pathways in 20 patients undergoing pancreaticoduodenectomy were analyzed. We injected ICG into the parenchyma in the anterior (n = 10) or posterior surface (n = 10) of the pancreas head and observed the intraoperative lymphatic flows by ICG fluorescence imaging. ***Results:*** The seven main lymphatic drainage pathways were identified: (1) along the anterior or posterior pancreaticoduodenal arcade, (2) running obliquely down behind the superior mesenteric vein (SMV), (3) reaching the left side of the superior mesenteric artery (SMA), (4) running longitudinally upward between the SMV and SMA, (5) along the middle colic artery toward the transverse colon, (6) reaching the paraaortic (PA) region, and (7) reaching the hepatoduodenal ligament. The lymphatic pathway reaching the left side of the SMA was observed in 4 patients (20%), while that reaching the PA region in 17 patients (85%). The mean time to reach around the SMA was longer than that to reach the PA region. ***Conclusions:*** We found that several lymphatic drainage routes were observed from the pancreatic head, suggesting that a lymphadectomy around the SMA might have a similar oncological impact as that of the PA region.

Introduction

Pancreatic cancer generally has a poor prognosis because the incidence of invasion of extrapancreatic fatty tissue, including lymphatic vessels and nerves, and distant metastasis is high [1–3]. The only chance of cure for pancreatic cancer is surgical resection followed by adjuvant chemotherapy [4]; however, the 5-year survival rate of patients undergoing curative resection remains a mere 7–25% [1–3]. Especially lymph node metastasis is the most important prognostic factor in the patients after surgical resection of pancreatic cancer [5–8]. Therefore, many surgeons have tried to perform an extended lymphadectomy as one strategy for improving survival in the patients with pancreatic cancer [9–12], since Fort-

KARGER
Fax +41 61 306 12 34
E-Mail karger@karger.ch
www.karger.com

0253–4886/12/0292–0132$38.00/0

Accessible online at:
www.karger.com/dsu

Hiroki Yamaue, MD
Second Department of Surgery
Wakayama Medical University School of Medicine
811-1 Kimiidera, Wakayama 641-8510 (Japan)
Tel. +81 73 441 0613, E-Mail yamaue-h@wakayama-med.ac.jp

ner [13] initially proposed 'regional pancreatectomy as en-bloc resection for pancreatic cancer with the lymphatic vessels and great vessels' in 1973. However, four prospective, randomized controlled studies were performed to analyze the potential advantage or disadvantage of an extended lymphadectomy in the patients with pancreatic head cancer, and it was suggested that the extended procedure did not benefit the overall survival, and there might even be a trend towards increased morbidity, including diarrhea and delayed gastric emptying [14–17].

Several reports have emphasized the importance of lymphadectomy along the superior mesenteric artery (SMA), including the first, second, and third jejunal arteries (J1, J2, and J3 regions) for locoregional control and improvement of survival in the patients with pancreatic head cancer [18–21]. They reported that the tissue adherent to the SMA might cause local recurrence after surgery, because the tissue contained the lymphatic structures from the uncinate process of the pancreas [22, 23], therefore they concluded that the circumferential clearance of the SMA, including J1, J2, and J3 regions, was needed in pancreatic head cancer [18, 19]. In all studies comparing the standard pancreatoduodenectomy (PD) and PD with extended lymphadectomy, extended lymphadectomy was focused on paraaortic (PA) lymph node dissection, but not lymph node dissection around the SMA, therefore no evidence was observed regarding the significance of the circumferential clearance of the SMA in pancreatic cancer.

Recently, an instrument providing fluorescence imaging of lymphatic flow, the photodynamic eye (PDE; Hamamatsu Photonics, Hamamatsu, Japan) [24], has been used in experimental and preliminary clinical studies for breast cancer and gastrointestinal cancer [25–28]. The indocyanine green (ICG) reagent is a 776-Da disulfonated small molecule and ICG absorbs light in the near-infrared range, with the maximum at a wavelength of 800 nm, and also emits maximal fluorescence at a wavelength of 840 nm when it binds to plasma proteins [29–32]. ICG fluorescence imaging has been reported to make it easy to distinguish lymphatic vessels and lymph nodes containing ICG particles from the surrounding tissue [24–28]. The PDE system, guided by ICG, can visualize the lymphatic drainage flow in the operating room in a real-time fashion [24–28].

The purpose of our study was to verify that extended lymphadectomy does not provide any substantial benefit regarding the locoregional control of pancreatic cancer, by visualizing the lymphatic pathway from the pancreatic head, using ICG fluorescence imaging. We first tried to identify the lymphatic pathways from the pancreatic head, by this new method using the PDE system, to analyze optimal lymphadectomy including that around the SMA basis on the lymphatic flows.

Materials and Methods

Patients

Our series consisted of 20 consecutive patients prospectively recruited who met the eligibility criteria of undergoing conventional pancreaticoduodenectomy (PD), pylorus-preserving PD (PpPD) or pylorus-resecting PD (PrPD) between October 2008 and June 2009 at Wakayama Medical University Hospital (WMUH).

The eligibility criteria were: (1) the maximum tumor diameter was <3 cm and located in the head of the pancreas, because massive cancerous invasion or intense desmoplastic reaction causes obstruction of the lymphatic vessels, and the dye would then be unable to follow the normal lymphatic flow, and (2) the age of the patients was <80 years. None of the patients received either chemotherapy or irradiation preoperatively. The procedures for this study were approved by the ethics committee of WMUH (No. 600), and written informed consent was obtained from each of the patients before he/she was included in this study.

Optimal Dose of ICG

To determine the optimal dose of ICG, we did the following: 25 mg of ICG (Diagnogreen; Daiichi Pharmaceutical, Tokyo, Japan) was diluted in a total of 5 ml. At first, the ability to observe lymphatic drainage was examined at 0.1 ml in 4 patients, but it was difficult to find the lymphatic flows with PDE in 2 of these patients (50%). Next, we checked the lymphatic drainage using 0.2 ml, and found that we could clearly observe the lymphatic flows that received ICG with PDF in all 4 patients (100%). Finally the ability to observe lymphatic drainage was examined at 0.4 ml. However, at this level, we could not distinguish lymphatic vessels from the surrounding adipose tissue, because ICG spread diffusely and was visualized as large shining fluorescent spots with PDE in 3 of the 4 patients (75%). On the basis of these results, we decided to inject 0.2 ml throughout the subsequent experiments using the 20 enrolled patients. Injection into the parenchyma in the anterior or posterior surface was alternately selected in the enrolled patients.

Technique

After laparotomy, Kocher's maneuver was performed carefully, and then gastric or duodenal resection was performed. A 0.2-ml aliquot of 0.5% ICG solution was injected into the parenchyma in the anterior or posterior surface of the uncinate process of the pancreas with a 26-gauge needle at a depth of 0.5 mm.

We observed intraoperative lymphatic drainage flows from the uncinate process of the pancreas by ICG fluorescence imaging using the PDE system. The fluorescence signals were transmitted to a digital video processor to be displayed on a TV monitor in real time. We assessed the pattern of spread of the ICG by the PDE for the initial 15 min after ICG injection, and also observed the

Table 1. Clinicopathological characteristics of the patients injected with ICG

No.	Age	Sex	Final histopathological diagnosis	Tumor size, cm	Operation	TNM stage[1]	Perineural invasion	Ratio of N+/N–
Patients injected with ICG into the anterior surface of the uncinate pancreas								
1	62	M	distal bile duct cancer	2.5	PrPD	T3, N1, M0; stage IIB	positive	2/11
2	77	F	distal bile duct cancer	1.2	PpPD	T3, N1, M0; stage IIB	positive	7/17
3	63	M	distal bile duct cancer	1.4	PrPD	T3, N0, M0; stage IIA	negative	0/13
4	69	M	pancreatic ductal adenocarcinoma	2.9	PrPD	T3, N1, M0; stage IIB	negative	2/13
5	70	F	pancreatic ductal adenocarcinoma	2.2	PrPD + SMV resection	T3, N1, M0; stage IIB	negative	1/33
6	61	F	pancreatic ductal adenocarcinoma	1.0	PrPD	T1, N0, M0; stage IA	negative	0/10
7	72	M	pancreatic ductal adenocarcinoma	2.8	PrPD + SMV resection	T3, N1, M0; stage IIB	negative	2/22
8	75	M	distal bile duct cancer	1.5	PpPD	T1, N1, M0; stage IIB	negative	4/21
9	58	F	chronic pancreatitis (tumor forming)	2.0	PrPD	–	–	–
10	67	F	pancreatic ductal adenocarcinoma	2.0	PD	T3, N0, M0; stage IIA	negative	0/11
Patients injected with ICG into the posterior surface of the uncinate pancreas								
11	69	F	pancreatic ductal adenocarcinoma	1.5	PpPD	T1, N0, M0; stage IA	negative	0/36
12	68	M	pancreatic ductal adenocarcinoma	2.3	PrPD	T3, N1, M0; stage IIB	negative	3/11
13	60	M	pancreatic ductal adenocarcinoma	1.8	PrPD	T3, N0, M0; stage IIA	negative	1/19
14	75	M	distal bile duct cancer	1.4	PrPD	T3, N1, M0; stage IIB	positive	1/29
15	65	F	pancreatic ductal adenocarcinoma	1.5	PpPD	T3, N0, M0; stage IIA	negative	0/14
16	75	F	pancreatic ductal adenocarcinoma	2.3	PrPD + SMV resection	T3, N1, M0; stage IIB	negative	2/27
17	71	M	pancreatic ductal adenocarcinoma	1.6	PrPD	T1, N1, M0; stage IIB	negative	2/15
18	79	F	distal bile duct cancer	1.3	PrPD	T3, N0, M0; stage IIA	negative	0/12
19	64	F	pancreatic ductal adenocarcinoma	1.0	PrPD	T1, N0, M0; stage IA	negative	0/12
20	53	M	pancreatic ductal adenocarcinoma	2.5	PrPD + SMV resection	T3, N1, M0; stage IIB	negative	4/45

[1] TNM classification of the Union internationale contre le cancer.

lymphatic flow at the time of resection of the bile duct (mean 50 min, range 29–110) and resection of the pancreas (mean 87 min, range 57–137). We performed sampling or dissection en bloc of tissue received ICG and then diagnosed these tissues in pathological examination.

Results

Patient Characteristics

Table 1 shows the clinicopathological characteristics of the patients in this study. The patients included 10 males and 10 females, with an average age of 68.2 ± 6.7 years (range 53–79). The final pathological diagnosis showed that 13 patients had pancreatic ductal adenocarcinoma, 6 had distal bile duct cancer, and 1 had tumor-forming pancreatitis. The mean size of the pancreatic tumors was 1.9 ± 0.6 cm (range 1.0–2.9). According to the UICC TNM classification [33], among 13 patients with pancreatic ductal carcinoma, 3 patients were stage IA, 3 patients were IIA, and 7 patients were stage IIB, while among the 6 patients with bile duct cancer, 2 patients were stage IIA and 4 patients were stage IIB. According to pathological examinations, 3 patients (15.8%) had perineural invasion and 10 patients (52.6%) had lymph node metastasis. 15 patients underwent PrPD, 4 PpPD, and 1 PD, and 4 patients also underwent a combined the superior mesenteric vein (SMV) resection.

Lymphatic Pathways from the Uncinate Process of the Pancreas and the Mean Time to Arrive at the Drainage Areas

There were no patients with complications or adverse events related to intraoperative injection of ICG, regardless of the dose (up to 0.4 ml). Immediately after the ICG injection, we were able to locate the lymphatic vessels draining the uncinate process of the pancreas as shining fluorescent streams and spots in fluorescence images of the PDE, whereas no lymphatic flow was clearly visible as green in color after ICG injection, and could not be easily judged as being lymphatic vessels by naked-eye examination.

The lymphatic drainage routes from the uncinate process of the pancreas detected with PDE are shown in tables 2 and 3. Seven main lymphatic pathways from the